

Exact numerical solution of the classical and quantum Heisenberg spin glass

Nikita Kavokine,^{1,2} Markus Müller,³ Antoine Georges,^{4,1,5,6} and Olivier Parcollet^{1,7}

¹*Center for Computational Quantum Physics, Flatiron Institute, 162 5th Avenue, New York, NY 10010, USA*

²*Department of Molecular Spectroscopy, Max Planck Institute for Polymer Research, Ackermannweg 10, 55128 Mainz, Germany*

³*Paul Scherrer Institut, CH-5232 Villigen PSI, Switzerland*

⁴*Collège de France, Université PSL, 11 place Marcelin Berthelot, 75005 Paris, France*

⁵*Centre de Physique Théorique, Ecole Polytechnique, CNRS, Institut Polytechnique de Paris, 91128 Palaiseau Cedex, France*

⁶*DQMP, Université de Genève, 24 quai Ernest Ansermet, CH-1211 Genève, Suisse*

⁷*Université Paris-Saclay, CNRS, CEA, Institut de Physique Théorique, 91191, Gif-sur-Yvette, France*

(Dated: January 12, 2024)

We present the mean field solution of the quantum and classical Heisenberg spin glasses, using the combination of a high precision numerical solution of the Parisi full replica symmetry breaking equations and a continuous time Quantum Monte Carlo. We characterize the spin glass order and its low-energy excitations down to zero temperature. The Heisenberg spin glass has a rougher energy landscape than its Ising analogue, and exhibits a very slow temperature evolution of its dynamical properties. We extend our analysis to the doped, metallic Heisenberg spin glass, which displays an unexpectedly slow spin dynamics reflecting the proximity to the melting quantum critical point and its associated Sachdev-Ye-Kitaev Planckian dynamics.

While the physics of classical and quantum Ising spin glasses has been rather thoroughly understood, glasses of Heisenberg (vector) spins have remained a difficult and largely unsolved problem, including especially its quantum version, which governs the local moments in randomly doped, strongly correlated materials.

The approach of Sachdev and Ye [1] (SY), which takes a double limit of a fully connected exchange model with $SU(2)$ spins promoted to $SU(M \gg 1)$, has attracted a lot of attention, as it exhibits very interesting features in the $M = \infty$ limit. In a fermionic representation of the $SU(M \rightarrow \infty)$ generators, the spins do not freeze, but remain in a spin liquid state [1] similarly to the closely related SYK model of randomly coupled Majorana fermions [2]. When expanding around $M = \infty$ it was conjectured that a transition into a glassy phase occurs at an exponentially small critical temperature $\log(T_g) \propto -\sqrt{M}$ [3], and a recent study has established that this phase displays full replica symmetry breaking (RSB) [4]. A glass phase with very similar features was previously found to occur in the transverse field Ising model [5, 6] and the related multi-component quantum rotor models [7–9]. In contrast, for bosonic $SU(M)$ representations, a spin glass phase occurs even for $M = \infty$, albeit with one-step RSB [3, 10].

There is a fundamental physical difference between glasses displaying full RSB and one-step RSB. The energy landscape of the former features marginally stable local minima with a gapless spectrum of excitations, while the latter display a fully stable, gapped ground-state, lying energetically far below the manifold of marginally stable excited states that trap the dynamics. Marginal stability is key to the dynamics and the physics of avalanches in full RSB systems [11]. Which of these two scenarios applies to the physically relevant Heisenberg $SU(2)$,

$S = 1/2$ spin-glass has remained an open question. Exact diagonalization of small fully connected systems is faced with strong finite size effects [12, 13]. Surprisingly, not much is known about the *classical* (large S) limit of the Heisenberg mean-field spin glass either, apart from the replica symmetric analysis of Refs. [14, 15].

The equilibrium quantum spin dynamics of the SY spin-liquid [1] is similar to that of a marginal Fermi liquid [16]. It was realized early on [17] that this opens a new perspective on ‘strange’ metals, culminating in recent models in which disorder and strong interactions conspire to prevent the emergence of quasiparticles and lead to T -linear resistivity down to the lowest temperatures (see e.g. [18], and [2] for a review). It has recently been shown that such a behavior is found in the quantum critical region around the melting point of a metallic $SU(2)$ Heisenberg spin glass [19, 20]. However, it is not known how the quantum dynamics change within the metallic spin-glass phase itself.

In this Letter, we answer these open questions and present a solution of the fully connected spin-1/2 Heisenberg spin-glass throughout its ordered phase. In the quantum case, the model reduces to a quantum impurity problem for the spin dynamics coupled to Parisi’s equations for the spin glass order. The Heisenberg glass has a full RSB solution, whose structure, however, differs crucially from an Ising glass. The insulating quantum glass displays the universal spin dynamics found in all solvable mean-field quantum glasses with full RSB in the limit $T \rightarrow 0$, but deviations from it persist to surprisingly low temperatures. Upon doping, we find a metallic spin glass with unexpectedly slow spin dynamics, close to the SY dynamics that dominate the quantum critical melting point of the spin glass.

Model and method. We consider N spins \mathbf{S}_i with all-to-all interactions, described by the Hamiltonian

$$\mathcal{H} = - \sum_{i < j} J_{ij} \mathbf{S}_i \cdot \mathbf{S}_j. \quad (1)$$

The \mathbf{S}_i are either classical Heisenberg spins – vectors constrained to the three-dimensional sphere of radius $S = 1/2$ – or quantum $SU(2)$ spins S (with $\mathbf{S}^2 = S(S+1)$). We use $\hbar = k_B = 1$ and denote by $\ell = 3$ the number of spin components. J_{ij} are Gaussian random couplings with zero mean and variance J^2/N . We obtain the equilibrium solution of this model using the replica method and Parisi's full RSB ansatz [21–24], as detailed in the Supplementary Information [25].

This mean field model may be reduced to an effective single spin problem in a random frozen field \mathbf{h} with distribution $\mathbb{P}(\mathbf{h})$. In the quantum case, the dynamics of this spin also depend on the self-averaging spin autocorrelation function $\chi(\tau) = \langle \mathbf{S}(0)\mathbf{S}(\tau) \rangle - \langle \mathbf{S} \rangle^2$, via the action

$$\begin{aligned} \mathcal{S}_{\text{loc}}(\mathbf{h}) = & \frac{J^2}{2} \iint_0^\beta d\tau d\tau' \chi(\tau - \tau') \mathbf{S}(\tau) \cdot \mathbf{S}(\tau') \\ & - \mathbf{h} \int_0^\beta d\tau \mathbf{S}(\tau), \end{aligned} \quad (2)$$

where τ is Matsubara imaginary time and $\beta = 1/T$ the inverse temperature. The glass phase is described by an ultrametric structure of metastable states, parametrized by Parisi's overlap function $q(x)$ ($x \in [0, 1]$) [24]. The local field distribution $\mathbb{P}(\mathbf{h}) \equiv \mathbb{P}(x=1, \mathbf{h})$ is found by solving Parisi's equations for the magnetization $\mathbf{s}(x, \mathbf{h})$ and frozen fields $\mathbb{P}(x, \mathbf{h})$

$$\frac{\partial \mathbf{s}}{\partial x} = - \frac{J^2}{2} \frac{dq}{dx} (\nabla^2 \mathbf{s} + 2\beta x (\mathbf{s} \cdot \nabla) \mathbf{s}), \quad (3a)$$

$$\frac{\partial \mathbb{P}}{\partial x} = \frac{J^2}{2} \frac{dq}{dx} (\nabla^2 \mathbb{P} - 2\beta x \nabla(\mathbf{s} \cdot \mathbb{P})), \quad (3b)$$

$$\mathbf{s}(1, \mathbf{h}) = \langle \mathbf{S} \rangle_{\mathcal{S}_{\text{loc}}(\mathbf{h})}, \quad (3c)$$

$$\mathbb{P}(0, \mathbf{h}) = \delta(\mathbf{h}). \quad (3d)$$

The overlap $q(x)$ satisfies

$$q(x) = \frac{1}{\ell} \int d\mathbf{h} \mathbb{P}(x, \mathbf{h}) \mathbf{s}(x, \mathbf{h})^2. \quad (4)$$

In the quantum case, χ is self-consistently given by

$$\chi(\tau) = \frac{1}{\ell} \int d\mathbf{h} \mathbb{P}(\mathbf{h}) \langle \mathbf{S}(0)\mathbf{S}(\tau) \rangle_{\mathcal{S}_{\text{loc}}(\mathbf{h})} - q(1). \quad (5)$$

These self-consistent equations for q, χ are an example of extended dynamical mean-field theory (EDMFT) [5, 26–28]. The iterative procedure to solve them is summarized in Fig. 1. A similar procedure has recently been implemented for mean field versions of transverse field Ising and quantum Coulomb glasses [6, 30]. In contrast

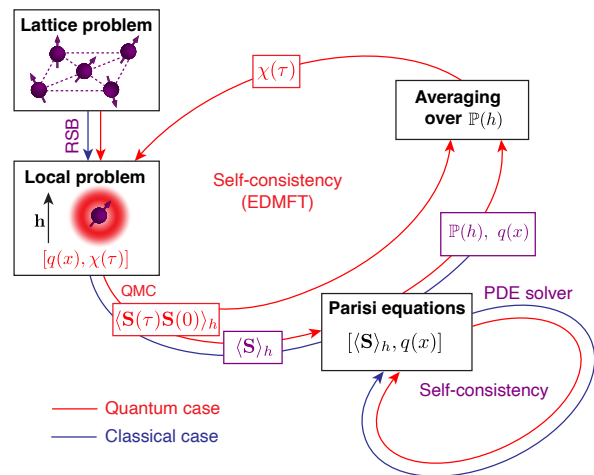


FIG. 1. Illustration of the algorithm to solve (2,3,4,5). In the classical case, the local problem is solved only once, and $q(x)$ is obtained solving Parisi's partial differential equations. In the quantum case, it is solved iteratively with CTQMC.

to the classical case, the single site quantum problem (2) cannot be solved analytically. Its solution is obtained with a "CTSEG" continuous-time quantum Monte Carlo (CTQMC) algorithm [25, 29], without fermionic sign problem. The Parisi equations are solved with a high precision numerical method (error bars on $q(x)$ being of order 10^{-5}), using their integral form [31] and filtering methods to suppress numerical instabilities at low T [25].

Glass phase. A spin glass phase appears below a critical temperature T_g , where the Edwards-Anderson order parameter $q_{\text{EA}} \equiv q(x=1)$ turns on, as illustrated on Fig. 2a. Our results for T_g are consistent with previous analytical work: $T_g = JS^2/3$ ($\approx 0.08J$ for $S^2 = 1/4$) in the classical case [32] and $T_g \approx J\langle \mathbf{S}^2 \rangle / 3\sqrt{3} \approx 0.15J$ in the quantum case [21], with $q_{\text{EA}}(T)$ following the prediction of [32] close to T_g (Fig. 2a, inset). Note that T_g is higher in the quantum case, since the quantum spins are larger ($S(S+1) > S^2$).

For $T \ll T_g$, the overlap function $q(x)$ obeys a scaling form $q(x, T) \approx q_{\text{EA}}(T)f(x/T)$ (Fig. 2a). Injecting this ansatz into the Parisi equations (3ab) allows us to solve them directly at $T = 0$. In the quantum case, they require as boundary conditions the zero temperature magnetizations, $\langle \mathbf{S}(\tau) \rangle_{\mathcal{S}_{\text{loc}}(\mathbf{h})}$, which we approximate by our lowest temperature QMC results (see [25] Fig. S5-S6). The results for $q(x)$ are shown in Figs. 2a,b. The maximal possible overlap is $q_{\text{max}} = \langle \mathbf{S}^2 \rangle / \ell$, corresponding to a product state without fluctuations. As expected, the classical glass approaches this value at $T = 0$, while quantum fluctuations weakly reduce the order parameter to $q_{\text{EA}} \approx 0.81q_{\text{max}}$ (consistent with exact diagonalization in Ref. [12], while the fit of spin correlations in Ref. [13] likely underestimated the order).

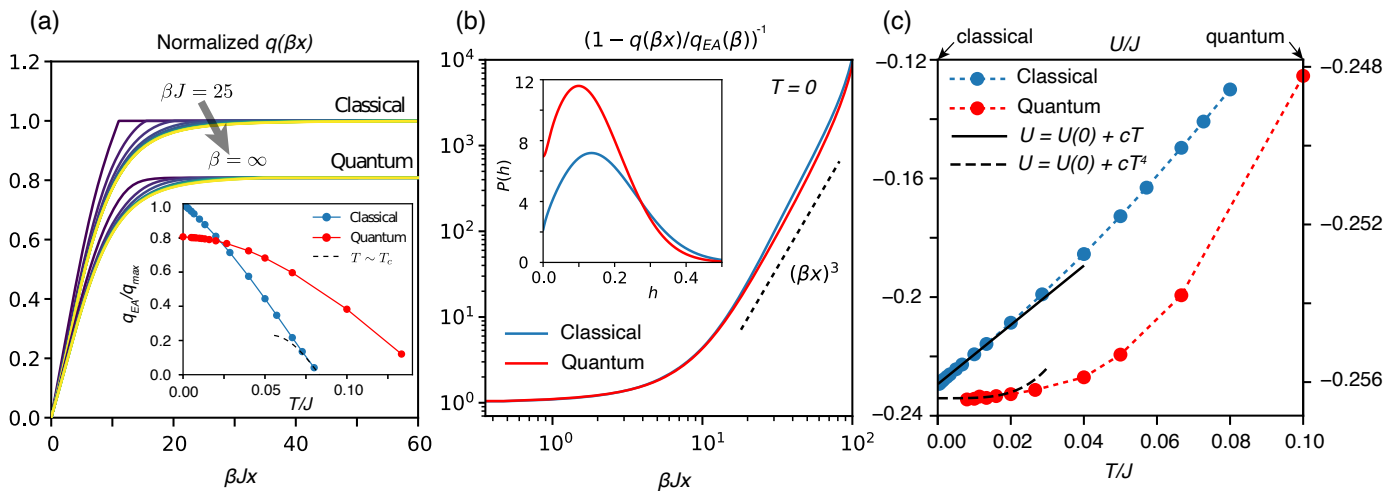


FIG. 2. **Characteristics of the glass phase.** (a) Overlap function $q(x)/q_{EA}(\beta)$, normalized by $q_{EA}(T=0)/q_{max}$, for a range of temperature values, from $\beta J = 25$ to $\beta = \infty$. At low enough temperature, $q(x)/q_{EA}(\beta)$ depends only on βx . Inset: q_{EA} vs T . The dashed line is the result of [32], valid for $T \approx T_g$. (b) $1 - q(x)/q_{EA}(T=0)$ at $T=0$, showing the power law approach to q_{EA} at large βx . Inset: local field distribution $\mathbb{P}(h)$ at zero temperature. (c) Internal energy as a function of temperature, with a fit for the classical case $U(T) - U(0) = cT$ ($c = 1 \pm 0.1$), and for the quantum case $U(T) - U(0) = cT^4$.

Unlike in the Ising case, local stability does not require a pseudogap in the distribution of local fields. Instead $\mathbb{P}(\mathbf{h} = 0)$ remains finite and $\mathbb{P}(h) \approx \mathbb{P}(0) + ah$ (cf. Fig. 2b), since the probability of dangerously small fields is already suppressed by the phase space factor $\sim h^{\ell-1}$ [33][14]. This in turn is related to the tail of the overlap function $q(x)$. Indeed, (4) suggests that for x close to 1, $q_{EA} - q(x)$ counts the number of spins that see frozen fields of order T/x , for which one may expect $q_{EA} - q(x) \sim \int_0^{T/x} dh h^2 \mathbb{P}(h) \sim (T/x)^3 + O(T/x)^4$, consistent with an apparent power law: $\sim (T/x)^\alpha$. Numerically we indeed find an apparent power law approach: $1 - q(x)/q_{EA} \sim 1/(\beta x)^\alpha$ as $T \rightarrow 0$, with α slightly larger than 3. This contrasts with the Ising case [5, 24, 33], where the linear pseudogap in $\mathbb{P}(h)$ leads to $\alpha = 2$. The lower density of small fields in the Heisenberg case suggests that low-lying metastable states have higher energies. This is consistent with the smaller value of the so-called breakpoint x_c , above which $q(x)$ reaches a plateau ([25], Fig. S12). $T/x_c(T)$ can be interpreted as the typical free energy difference between the lowest metastable states [34]. While in the Ising case that energy scales linearly with T as $x_c(T \rightarrow 0) \approx 0.5$ [33], in Heisenberg glasses it decreases much more slowly as $T/x_c(T) \sim 1/\log(1/T)$, corroborating the picture of a rougher energy landscape. These differences will further show in the response to an increasing external field, under which the ground state magnetization increases in random discontinuous steps called ‘shocks’. Their size distribution $\rho(\Delta m)$ was numerically found to be very similar to that of field-triggered out-of-equilibrium avalanches in the classical SK model [35, 36], a phenomenon attributed to the marginal stability of the full RSB land-

scape. The equilibrium $\rho(\Delta m)$ is governed by the asymptotic approach of $q(x)$ to q_{EA} . If it scales as $(T/x)^\alpha$, then $\rho(\Delta m) \sim 1/(\Delta m)^{2/\alpha}$ for $N^{-1/2} \ll \Delta m \ll 1$ [36]. For the classical Ising glass with $\alpha = 2$, $\rho(\Delta m) \propto 1/(\Delta m)$ exhibits a broad spectrum of avalanches. The larger $\alpha \approx 3$ of Heisenberg glasses leads to $\rho(\Delta m) \propto 1/(\Delta m)^{2/3}$, with predominant large scale rearrangements – as numerically observed in avalanches of XY ($\ell = 2$) spins. [37]

Specific heat. Let us now consider the internal energy per spin. In the classical case, it is given by [25]:

$$U_{Cl} = -\frac{\beta J^2 S^4}{2\ell} \left(1 - \frac{\ell^2}{S^4} \int_0^1 dx q(x)^2 \right). \quad (6)$$

In the quantum case, denoting $Q(\tau) = \chi(\tau) + q_{EA}$ and $\bar{\tau} = \tau/\beta$, it reads

$$U_Q = -\frac{\ell \beta J^2}{2} \left(\int_0^1 d\bar{\tau} Q(\bar{\tau})^2 - \int_0^1 dx q(x)^2 \right). \quad (7)$$

As shown in Fig. 2c, the classical and quantum internal energies behave very differently as a function of temperature. For classical vector spins, one expects a constant intra-state heat capacity $c = (\ell - 1)/2$ as $T \rightarrow 0$, each degree of freedom contributing 1/2 by the equipartition theorem. A linear fit to our data yields $c \approx 1.0 \pm 0.1$, excluding sizeable inter-state contributions, consistent with finite-size simulations [38]. Quantum effects gap out most of the soft degrees of freedom and yield a much weaker temperature dependence of the internal energy (Fig. 2c). Our data are compatible with $U(T) \propto T^4$, but only at the lowest temperatures $T/J \lesssim 0.02$, as finite temperature corrections are substantial. This result is similar to several examples of quantum spin glasses solved by 1-

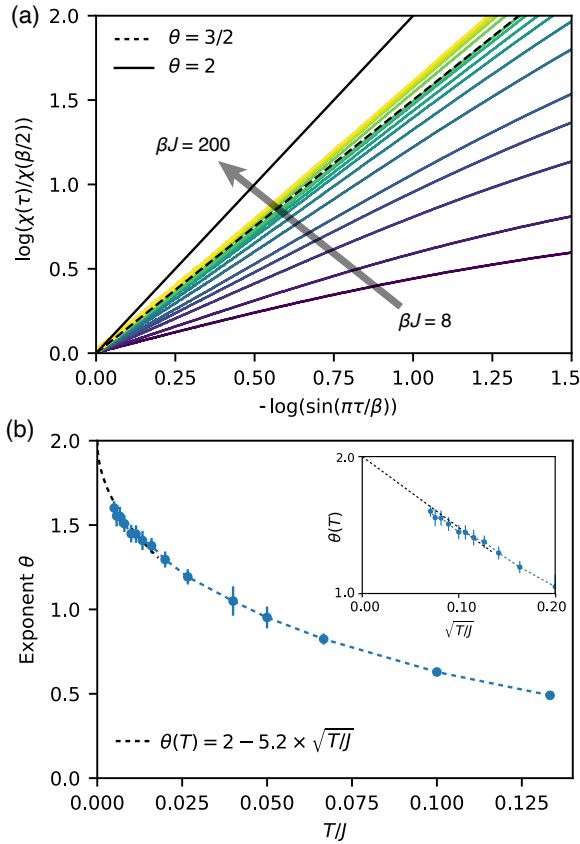


FIG. 3. **Spin susceptibility.** (a) Rescaled spin autocorrelation function in imaginary time, $\chi(\tau)/\chi(\beta/2)$, for a range of temperatures (from $\beta J = 8$ to $\beta J = 200$). At low temperature, it is well described by the conformal scaling form $\chi(\tau)/\chi(\beta/2) \approx [1/\sin(\pi\tau/\beta)]^\theta$, as shown by the linear behavior in the logarithmic plot. (b) Exponent θ , obtained by fitting $Q(\tau)$ with the conformal scaling form, as a function of temperature. Inset: θ as a function of $\sqrt{T/J}$. The data is well described by $\theta(T) = 2 - 5.2 \times \sqrt{T/J}$ (black dashed line).

step RSB where $c \propto T^3$ (provided that marginally stable rather than equilibrium states are analyzed) [39].

Spin susceptibility. The spin-spin correlator $\chi(\tau)$ is shown in Fig. 3a. For large τ it is well described by the conformal scaling form $\chi(\tau) \approx \chi(\beta/2)/[\sin(\pi\tau/\beta)]^\theta$ [17], implying that for $\omega \gtrsim T$, the dissipative part of the susceptibility at real frequencies $\chi''(\omega)$ scales as $\omega^{\theta-1}$. The exponent θ has significant, slow T -dependence (Fig. 3b). Using a Landau expansion, Ref. [8] predicted that $\theta(T=0) = 2$, ($\chi''(\omega) \propto \omega$). This value was also found in a $1/M$ expansion of the $SU(M)$ quantum spin glass [4] and actually holds for all solvable cases of marginally stable states found so far [40]. From the limited numerically accessible temperature range, it is hard to unambiguously conclude whether $\lim_{T \rightarrow 0} \theta(T) = 2$. However, Fig. 3b suggests that this limit is indeed approached, albeit very slowly, as we can fit our data by $\theta(T) \approx 2 - 5.2 \times \sqrt{T/J}$. Interestingly, a similar behavior was found recently in the

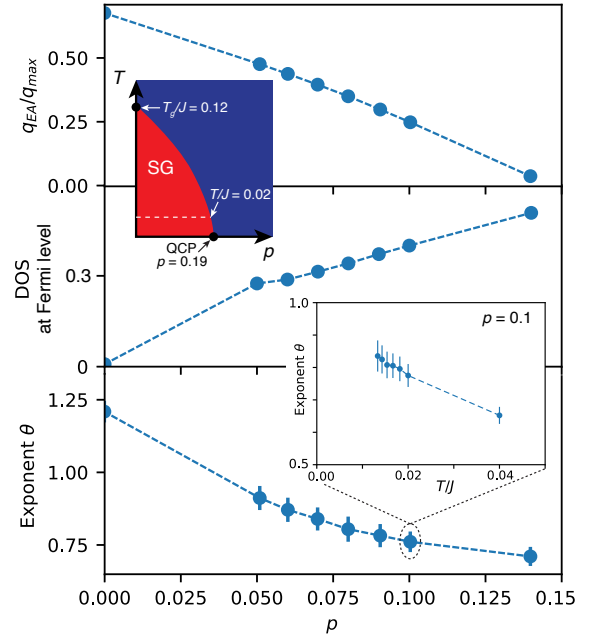


FIG. 4. **Doped case.** Glass order parameter q_{EA} , density of states at the Fermi level, and scaling exponent θ of the spin-spin correlation function, as a function of doping p at $\beta J = 50$. Upper inset: sketch of phase diagram. The spin glass (SG) melts at the quantum critical point (QCP). Lower inset: θ at fixed doping $p = 0.1$, as a function of temperature.

transverse-field Ising spin glass [6].

As discussed in Refs. [5, 40], the low- T behavior $c \propto T^3$, $\chi''(\omega) \propto \omega$ ($\theta = 2$) can be physically rationalized by approximating the eigenmodes of the Hessian describing the local curvature of the energy landscape as independent oscillators with spring constants λ distributed as the eigenvalues of a random matrix $\rho(\lambda) \sim \sqrt{\lambda}$. For undamped oscillators of mass M , one has $M\omega^2 \sim \lambda$ with zero-point amplitudes given by $\lambda \langle x^2 \rangle_\omega \sim \hbar\omega$, leading to $\chi''(\omega) \sim \rho(\omega) \langle x^2 \rangle_\omega \sim \sqrt{M}\omega$. In this picture, an effective exponent $\theta < 2$ at finite T may result from a T -dependent friction among modes. It may also indicate that interactions between modes are significant at finite- T , but become irrelevant in the $T = 0$ limit. Assuming $\lim_{T \rightarrow 0} \theta(T) = 2$, we have $A \equiv \lim_{\omega \rightarrow 0} \chi''(\omega)/\omega \approx \lim_{\beta \rightarrow \infty} \beta^2 \chi(\beta/2)/\pi$. We find $A \approx 3.5J^2$ and thus a significantly larger density of soft excitations than in the transverse field Ising spin glass, where $A \sim 0.5J^2$ (independent of the transverse field) was reported [5, 6].

Metallic quantum spin glass. In order to study the interplay between electrons and frozen spins arising from doping the spin glass, we use the Hamiltonian:

$$\mathcal{H} = - \sum_{ij, \sigma=\uparrow, \downarrow} t_{ij} c_{i\sigma}^\dagger c_{j\sigma} + U \sum_i n_{i\uparrow} n_{i\downarrow} - \sum_{i < j} J_{ij} \mathbf{S}_i \cdot \mathbf{S}_j, \quad (8)$$

where $c_{i\sigma}$ and $c_{i\sigma}^\dagger$ are the electronic annihilation and creation operators, $n_{i\sigma} = c_{i\sigma}^\dagger c_{i\sigma}$, $\mathbf{S}_i^a = c_{i\sigma}^\dagger \sigma_{\sigma\sigma'}^a c_{i\sigma'}$ and U

is the on-site electron-electron interaction. The hopping amplitudes t_{ij} are randomly distributed with variance t^2/N . We denote the doping by $p = \langle n_\uparrow + n_\downarrow \rangle - 1$. This model has previously been solved in the paramagnetic phase [20]. Here, we solve the spin glass phase; as in [20], we use $U = 4t$ and $J = 0.5t$.

Below a critical doping p_c , a metallic spin glass appears, *i.e.* a phase with both a non-zero spin glass order parameter q_{EA} and a non-zero density of states at zero frequency, as illustrated in Fig. 4. This is compatible with the spin glass instability of the paramagnetic solution found in [20]. Previous studies of metallic quantum spin glasses have found a local spin susceptibility $\chi''(\omega) \propto \sqrt{\omega}$ corresponding to an exponent $\theta = 3/2$ at $T = 0$ [26, 40, 41]. This can be interpreted as originating from Ohmic damping of the oscillators in the physical picture discussed above. Intriguingly, we find that θ is smaller than unity for the whole range of (low) temperatures investigated. Our data do not appear consistent with θ reaching $3/2$ at $T = 0$ (possibly due to non-Ohmic damping by the non-Fermi-liquid metal) but may be consistent with θ reaching 1. The latter corresponds to the quantum critical dynamics found at the critical point $p = p_c$, which might extend through a large part of the metallic spin-glass phase.

In conclusion, we have solved the Heisenberg quantum spin glass for $SU(2)$ spins. We found that the glassy energy landscape of vector spins differs significantly from the Ising counterpart, resulting in different long time dynamics. Upon decreasing T , the short time quantum dynamics slowly approach the super-universal behavior of marginal mean field glasses, although featuring significantly softer collective modes and a lower freezing temperature than comparable Ising glasses. The marginal Fermi liquid-type quantum dynamics anticipated from the $SU(M \gg 1)$ approach is essentially absent in the undoped insulating limit of $SU(2)$ spins, but appears to be present in a wide window influenced by the doping-induced quantum critical point in a metallic regime, that may be relevant for strongly correlated doped materials.

The data and code associated with the paper are publicly available [42, 43]. We thank Philipp Dumitrescu, Subir Sachdev and Nils Wentzell for fruitful discussions. The Flatiron Institute is a division of the Simons Foundation. N.K. acknowledges support from a Humboldt fellowship.

[1] S. Sachdev and J. Ye, Phys. Rev. Lett. **70**, 3339 (1993).
 [2] D. Chowdhury, A. Georges, O. Parcollet, and S. Sachdev, Rev. Mod. Phys. **94**, 035004 (2022).
 [3] A. Georges, O. Parcollet, and S. Sachdev, Phys. Rev. B **63**, 1344061 (2001).
 [4] M. Christos, F. M. Haehl, and S. Sachdev, Phys. Rev. B **105**, 085120 (2022).

[5] A. Andreanov and M. Müller, Phys. Rev. Lett. **109**, 177201 (2012).
 [6] A. Kiss, G. Zaránd, and I. Lovas, (2023), arXiv:2306.07337.
 [7] J. Ye, S. Sachdev, and N. Read, Phys. Rev. Lett. **70**, 4011 (1993).
 [8] N. Read, S. Sachdev, and J. Ye, Phys. Rev. B **52**, 384 (1995).
 [9] M. Tikhanovskaya, S. Sachdev, and R. Samajdar, “Equilibrium dynamics of infinite-range quantum spin glasses in a field,” (2023), arXiv:2309.03255.
 [10] A. Georges, O. Parcollet, and S. Sachdev, Phys. Rev. Lett. **85**, 840 (2000).
 [11] M. Müller and M. Wyart, Annual Review of Condensed Matter Physics **6**, 177 (2015).
 [12] L. Arrachea and M. J. Rozenberg, Phys. Rev. Lett. **86**, 5172 (2001).
 [13] H. Shackleton, A. Wietek, A. Georges, and S. Sachdev, Phys. Rev. Lett. **126**, 136602 (2021).
 [14] A. J. Bray and M. A. Moore, J. Phys. C: Solid State Phys. **14**, 2629 (1981).
 [15] S. Franz, F. Nicoletti, G. Parisi, and F. Ricci-Tersenghi, SciPost Phys. **12**, 016 (2022).
 [16] C. M. Varma, P. B. Littlewood, S. Schmitt-Rink, E. Abrahams, and A. E. Ruckenstein, Phys. Rev. Lett. **63**, 1996 (1989).
 [17] O. Parcollet and A. Georges, Phys. Rev. B **59**, 5341 (1999).
 [18] A. A. Patel, H. Guo, I. Esterlis, and S. Sachdev, Science **381**, 790 (2023).
 [19] P. Cha, N. Wentzell, O. Parcollet, A. Georges, and E. A. Kim, PNAS **117**, 18341 (2020).
 [20] P. T. Dumitrescu, N. Wentzell, A. Georges, and O. Parcollet, Phys. Rev. B **4**, L180404 (2022).
 [21] A. J. Bray and M. A. Moore, J. Phys. C: Solid State Phys. **13**, L655 (1980).
 [22] G. Parisi, J. Phys. A: Math. Gen. **13**, L115 (1980).
 [23] B. Duplantier, J. Phys. A: Math. Gen. **14**, 283 (1981).
 [24] M. Mézard, G. Parisi, and M. A. Virasoro, “Spin Glass Theory and Beyond,” (World Scientific, 1987) Chap. 3.
 [25] See Supplemental Material.
 [26] A. M. Sengupta and A. Georges, Phys. Rev. B **52**, 10295 (1995).
 [27] J. L. Smith and Q. Si, Phys. Rev. B **61**, 5184 (2000).
 [28] R. Chitra and G. Kotliar, Phys. Rev. Lett. **84**, 3678 (2000).
 [29] J. Otsuki, Phys. Rev. B **87**, 125102 (2013).
 [30] I. Lovas, A. Kiss, C. Pascu Moca, and G. Zaránd, Phys. Rev. Research **4**, 023067 (2022).
 [31] K. Nemoto, J. Phys. C: Solid State Phys. **20**, 1325 (1987).
 [32] M. Gabay, T. Garel, and C. De Dominicis, J. Phys. C: Solid State Phys. **15**, 7165 (1982).
 [33] A. Crisanti and T. Rizzo, Physical Review E **65**, 9 (2002).
 [34] M. Mézard, G. Parisi, and M. A. Virasoro, “Spin Glass Theory and Beyond,” (World Scientific, 1987) Chap. 4.
 [35] F. Pázmándi, G. Zaránd, and G. T. Zimányi, Phys. Rev. Lett. **83**, 1034 (1999).
 [36] P. Le Doussal, M. Müller, and K. J. Wiese, EPL **91**, 57004 (2010).
 [37] A. Sharma, A. Andreanov, and M. Müller, Phys. Rev. E **90**, 042103 (2014).
 [38] W. Ching and D. Huber, Physics Letters A **59**, 383 (1976).
 [39] G. Schehr, Phys. Rev. B **71**, 184204 (2005).

- [40] L. F. Cugliandolo and M. Müller, “Spin glass theory and far beyond,” (World Scientific, 2023) Chap. 18 - Quantum Glasses – a review.
- [41] S. Sachdev, N. Read, and R. Oppermann, Phys. Rev. B **52**, 10286 (1995).
- [42] https://github.com/TRIQS/ctseg_J.
- [43] DOI: 10.5281/zenodo.10475973.

Supplementary Information for:

Exact numerical solution of the classical and quantum Heisenberg spin glass

Nikita Kavokine, Markus Müller, Antoine Georges and Olivier Parcollet

-

Contents

1	Solution of the mean-field Heisenberg spin glass	1
1.1	Model definition	1
1.2	Replica trick	1
1.3	Replica symmetry breaking	4
1.4	Internal energy	9
1.5	Doped quantum spin glass	10
2	Numerical procedures	12
2.1	Solution of the Parisi equations	12
2.2	Solution of the quantum impurity problem	13
2.3	General solution procedure	13
3	Supplementary figures	15

arXiv:2312.14598v2 [cond-mat.dis-nn] 11 Jan 2024

1 Solution of the mean-field Heisenberg spin glass

In this section, we describe the analytical procedure that reduces the mean-field (infinite dimensional) Heisenberg spin glass problem to a self-consistent single spin problem, amenable to an exact numerical solution. We make use of the replica method, as introduced by Sherrington and Kirkpatrick in the classical case [1] and by Bray and Moore in the quantum case [2]. We then follow Parisi's seminal replica symmetry breaking construction [3, 4], which was generalized to the quantum case of the transverse field Sherrington-Kirkpatrick model [5, 6], but not to the quantum Heisenberg spin glass.

1.1 Model definition

We consider an all-to-all interacting system of N spins \mathbf{S}_i , described by the Hamiltonian

$$H = - \sum_{i < j} J_{ij} \mathbf{S}_i \cdot \mathbf{S}_j. \quad (1)$$

The J_{ij} are independent random variables with distribution $\mathbb{G}(J_{ij}|J^2/N)$, where $\mathbb{G}(x|v)$ is the normalized Gaussian with zero mean and variance v . We will consider both a classical and a quantum version of the model. In the classical case, the \mathbf{S}_i are vectors constrained to reside on the ℓ -dimensional sphere of radius S . In the quantum case, the \mathbf{S}_i are operators, forming a representation of spin S of the group $SU(2)$; we denote $\ell = 3$ the number of spin components.

1.2 Replica trick

Our aim is to compute f , the thermodynamic limit of the free energy per site at inverse temperature β . To this end, we introduce the quantity $f_n(N) \equiv (-1/\beta N) \log(\overline{Z^n})$, where the bar denotes averaging over the disorder. Z^n is the partition function of n replicas of the N -spin system, with the same realization of the disorder. Allowing n to take non-integer values through analytical continuation, we find

$$\frac{f_n(N)}{n} = - \frac{1}{\beta n N} \log \left(\overline{e^{n \log Z}} \right) \underset{n \rightarrow 0}{=} - \frac{1}{\beta N} \overline{\log Z}. \quad (2)$$

Since the free energy is self-averaging in the thermodynamic limit,

$$f = \lim_{N \rightarrow \infty} \lim_{n \rightarrow 0} \frac{f_n(N)}{n}. \quad (3)$$

We will assume that the order of the limits can be reversed, and first carry out the computation of f_n in the thermodynamic limit.

1.2.1 Classical case

We average over the random couplings the partition function of n replicas of the spin system, labeled by the index a :

$$\overline{Z^n} = \sum_{\{\mathbf{S}_i^a\}} \int_{-\infty}^{+\infty} \prod_{i < j} dJ_{ij} \mathbb{G}(J_{ij}|J^2/N) \exp \left[\beta \sum_a \sum_{i < j} J_{ij} \mathbf{S}_i^a \cdot \mathbf{S}_j^a \right] \quad (4)$$

$$= \sum_{\{\mathbf{S}_i^a\}} \exp \left[\frac{\beta^2 J^2}{2N} \sum_{i < j} \sum_{a,b} (\mathbf{S}_i^a \cdot \mathbf{S}_j^a) (\mathbf{S}_i^b \cdot \mathbf{S}_j^b) \right] \quad (5)$$

$$= \sum_{\{\mathbf{S}_i^a\}} \exp \left[\frac{\beta^2 J^2}{4N} \sum_{\alpha, \beta} \sum_{a,b} \left(\sum_i S_{i,\alpha}^a \cdot S_{i,\beta}^b \right)^2 - n^2 \frac{\beta^2 J^2 N S^4}{4} \right]. \quad (6)$$

Here, the indices α, β denote the spin components. We may drop in the following the term proportional to n^2 , since it vanishes in the $n \rightarrow 0$ limit. We now perform a Hubbard-Stratonovitch transformation to decouple the sum over spins:

$$\overline{Z}^n = \int \prod_{a,b,\alpha,\beta} \frac{dQ_{ab}^{\alpha\beta}}{\sqrt{4\pi/(N\beta^2 J^2)}} e^{-N\mathcal{F}\{Q_{ab}^{\alpha\beta}\}}, \quad (7)$$

with

$$\mathcal{F}\{Q_{ab}^{\alpha\beta}\} = \frac{\beta^2 J^2}{4} \sum_{a,b} \sum_{\alpha,\beta} (Q_{ab}^{\alpha\beta})^2 - \log \left[\sum_{\{\mathbf{S}^a\}} \exp \left(\frac{\beta^2 J^2}{2} \sum_{a,b} \sum_{\alpha,\beta} Q_{ab}^{\alpha\beta} S_\alpha^a \cdot S_\beta^b \right) \right]. \quad (8)$$

In the thermodynamic limit, the integral in Eq. (7) is dominated by the saddle point $\{Q_{ab}^{\alpha\beta*}\}$:

$$f_n(N) = (-1/\beta N) \log(\overline{Z}^n) \xrightarrow{N \rightarrow \infty} \frac{1}{\beta} \mathcal{F}\{Q_{ab}^{\alpha\beta*}\}, \quad (9)$$

with $\partial\mathcal{F}/\partial Q_{ab}^{\alpha\beta} |_{Q_{ab}^{\alpha\beta*}} = 0, \forall(a, b, \alpha, \beta)$. The latter amounts to

$$Q_{ab}^{\alpha\beta*} = \langle S_\alpha^a \cdot S_\beta^b \rangle_{H_{\text{loc}}[Q^*]}, \quad H_{\text{loc}}[Q^*] = -\frac{\beta J^2}{2} \sum_{a,b} \sum_{\alpha,\beta} Q_{ab}^{\alpha\beta*} S_\alpha^a \cdot S_\beta^b. \quad (10)$$

1.2.2 Quantum case

In the quantum case, we use an imaginary time path integral formalism to express the partition function:

$$\overline{Z}^n = \sum_{\{\mathbf{S}_i^a\}} \int_{-\infty}^{+\infty} \prod_{i<j} dJ_{ij} \mathbb{G}(J_{ij}|J^2/N) \exp \left[\beta \sum_a \sum_{i<j} J_{ij} \int_0^1 d\tau \mathbf{S}_i^a(\tau) \cdot \mathbf{S}_j^a(\tau) \right], \quad (11)$$

where the notation $\sum_{\mathbf{S}}[\cdot]$ is now taken to mean the path integral $\int [D\mathbf{S}(\tau)] e^{-S_0[\mathbf{S}(\tau)]}[\cdot]$, where $S_0[\mathbf{S}(\tau)]$ is the imaginary time action describing an isolated spin, which we do not need to specify explicitly. We may then proceed as in the classical case:

$$\overline{Z}^n = \sum_{\{\mathbf{S}_i^a\}} \exp \left[\frac{\beta^2 J^2}{2N} \int_0^1 d\tau d\tau' \sum_{i<j} \sum_{a,b} (\mathbf{S}_i^a(\tau) \cdot \mathbf{S}_j^a(\tau')) (\mathbf{S}_i^b(\tau) \cdot \mathbf{S}_j^b(\tau')) \right] \quad (12)$$

$$= \sum_{\{\mathbf{S}_i^a\}} \exp \left[\frac{\beta^2 J^2}{4N} \int_0^1 d\tau d\tau' \sum_{\alpha,\beta} \sum_{a,b} \left(\sum_i S_{i,\alpha}^a(\tau) \cdot S_{i,\beta}^b(\tau') \right)^2 - n^2 \frac{\beta^2 J^2 N}{4} S^2 (S+1)^2 \right] \quad (13)$$

We may again drop the term proportional to n^2 as it vanishes in the $n \rightarrow 0$ limit. The Hubbard-Stratonovitch transformation yields

$$\overline{Z}^n = \int \prod_{a,b,\alpha,\beta} \int_0^1 d\tau d\tau' \frac{dQ_{ab}^{\alpha\beta}(\tau, \tau')}{\sqrt{4\pi/(N\beta^2 J^2)}} e^{-N\mathcal{F}\{Q_{ab}^{\alpha\beta}(\tau, \tau')\}}, \quad (14)$$

with

$$\begin{aligned} \mathcal{F}\{Q_{ab}\} = & \frac{\beta^2 J^2}{4} \int_0^1 d\tau d\tau' \sum_{a,b} \sum_{\alpha,\beta} (Q_{ab}^{\alpha\beta}(\tau, \tau'))^2 \\ & - \log \left[\sum_{\{\mathbf{S}^a\}} \exp \left(\frac{\beta^2 J^2}{2} \int_0^1 d\tau d\tau' \sum_{a,b} \sum_{\alpha,\beta} Q_{ab}^{\alpha\beta}(\tau, \tau') S_\alpha^a(\tau) \cdot S_\beta^b(\tau') \right) \right]. \end{aligned} \quad (15)$$

The saddle point approximation in the thermodynamic limit yields

$$f_n(N) = (-1/\beta N) \log(\overline{Z^n}) \xrightarrow{N \rightarrow \infty} \frac{1}{\beta} \mathcal{F}[\{Q_{ab}^{\alpha\beta^*}(\tau, \tau')\}], \quad (16)$$

with $\partial \mathcal{F} / \partial Q_{ab}^{\alpha\beta^*}(\tau, \tau')|_{Q_{ab}^{\alpha\beta^*}(\tau, \tau')} = 0, \forall(a, b, \alpha, \beta, \tau, \tau')$. The latter amounts to

$$Q_{ab}^{\alpha\beta^*}(\tau, \tau') = \langle \text{T} S_\alpha^a(\tau) \cdot S_\beta^b(\tau') \rangle_{\mathcal{S}_{\text{loc}}[Q^*]}, \quad (17)$$

$$\mathcal{S}_{\text{loc}}[Q^*] = \sum_a \mathcal{S}_0[\mathbf{S}^a(\tau)] - \frac{\beta^2 J^2}{2} \int_0^1 d\tau d\tau' \sum_{a,b} \sum_{\alpha,\beta} Q_{ab}^{\alpha\beta^*}(\tau, \tau') S_\alpha^a(\tau) \cdot S_\beta^b(\tau'). \quad (18)$$

1.2.3 Interpretation of the Q_{ab}

We have reduced the initial lattice problem to a self-consistent local problem of n coupled replicas in the limit $n \rightarrow 0$, which remains to be defined. We now establish the link between the spin-spin correlation functions of the local problem and those of the initial lattice problem. This will allow us to simplify some of the coefficients Q_{ab} that define the local problem. For generality, we present here the reasoning in the quantum case.

Let \mathcal{S} be the action corresponding to the initial lattice problem. We supplement it with a source term:

$$\mathcal{S} \mapsto \mathcal{S} + \beta^2 h \int_0^1 d\tau d\tau' \sum_i S_{i\alpha}(\tau) S_{i\beta}(\tau'). \quad (19)$$

Then, in the thermodynamic limit,

$$\begin{aligned} \int_0^1 d\tau d\tau' \overline{\langle \text{T} S_{i\alpha}(\tau) S_{i\beta}(\tau') \rangle}_{\mathcal{S}} &= \partial f / \partial h|_{h=0} \\ &= \lim_{n \rightarrow 0} \partial(f_n(N \rightarrow \infty)/n) / \partial h|_{h=0} \\ &= - \lim_{n \rightarrow 0} \frac{1}{n} \frac{\partial}{\partial h} \Big|_{h=0} \log \sum_{\{\mathbf{S}^a\}} e^{-\mathcal{S}_{\text{loc}}[Q^*] - h \int_0^1 d\tau d\tau' \sum_a S_\alpha^a(\tau) S_\beta^a(\tau')} \\ &= \lim_{n \rightarrow 0} \frac{1}{n} \sum_a \int_0^1 d\tau d\tau' \langle \text{T} S_\alpha^a(\tau) S_\beta^a(\tau') \rangle_{\mathcal{S}_{\text{loc}}[Q^*]} \\ &= \lim_{n \rightarrow 0} \int_0^1 d\tau d\tau' \langle \text{T} S_\alpha^a(\tau) S_\beta^a(\tau') \rangle_{\mathcal{S}_{\text{loc}}[Q^*]}. \end{aligned} \quad (20)$$

Since the correlation function on the left hand side vanishes for two different spin components, the $Q_{aa}^{\alpha\beta^*}$ vanish if $\alpha \neq \beta$. We then set $Q(\tau - \tau') \equiv Q_{aa}^{\alpha\beta^*}(\tau, \tau')$. Consider now two copies of the initial system, governed by the action

$$\mathcal{S}_{\text{II}} = \mathcal{S}[\{\mathbf{S}_i^1\}] + \mathcal{S}[\{\mathbf{S}_i^2\}] \quad (21)$$

By applying the replica method to this action in the same way as above, we find the correspondence

$$\overline{\langle \text{T} S_{i\alpha}^1(\tau) S_{i\beta}^2(\tau') \rangle}_{\mathcal{S}_{\text{II}}} = \lim_{n \rightarrow 0, a \neq b} \langle \text{T} S_\alpha^a(\tau) S_\beta^b(\tau') \rangle_{\mathcal{S}_{\text{loc}}[Q^*]} \quad (22)$$

As the copies 1 and 2 are independent, the right hand side of the above equation, and therefore the $Q_{ab}^{\alpha\beta^*}, a \neq b$, cannot depend on τ, τ' . Similarly, in the absence of quadrupolar order in the initial system, the $Q_{ab}^{\alpha\beta^*}$ vanish when $a \neq b$ and $\alpha \neq \beta$. The reasoning is analogous in the classical case. Thanks to the normalization of the classical spins, Eq. (8) may be further simplified by integrating over the $Q_{aa}^{\alpha\alpha}$ in Eq. (7).

Let us summarize our results so far.

In the classical case, the free energy per spin is

$$f = -\frac{\beta J^2 S^4}{4\ell} + \lim_{n \rightarrow 0} \frac{1}{\beta n} \left[\frac{\ell \beta^2 J^2}{2} \sum_{a < b} Q_{ab}^2 - \log Z_{\text{loc}}^{\text{Cl}} \right], \quad (23)$$

with

$$Z_{\text{loc}}^{\text{Cl}} = \sum_{\{\mathbf{S}^a\}} e^{-\beta H_{\text{loc}}}, \quad Q_{ab} = \frac{1}{\ell} \langle \mathbf{S}^a \cdot \mathbf{S}^b \rangle_{H_{\text{loc}}}, \quad H_{\text{loc}} = -\beta J^2 \sum_{a < b} Q_{ab} \mathbf{S}^a \cdot \mathbf{S}^b. \quad (24)$$

In the quantum case,

$$f = \frac{\ell \beta J^2}{4} \int_0^1 d\tau Q(\tau)^2 + \lim_{n \rightarrow 0} \frac{1}{\beta n} \left\{ \frac{\ell \beta^2 J^2}{2} \sum_{a < b} Q_{ab}^2 - \log Z_{\text{loc}}^{\text{Q}} \right\}, \quad (25)$$

with

$$Z_{\text{loc}}^{\text{Q}} = \int \prod_a [D\mathbf{S}^a(\tau)] e^{-S_{\text{loc}}}, \quad Q_{ab} = \frac{1}{\ell} \langle \text{T} \mathbf{S}^a(\tau) \cdot \mathbf{S}^b(\tau') \rangle_{S_{\text{loc}}}, \quad Q(\tau) = \frac{1}{\ell} \langle \text{T} \mathbf{S}^a(\tau) \cdot \mathbf{S}^a(0) \rangle_{S_{\text{loc}}}, \quad (26)$$

and

$$S_{\text{loc}} = \sum_a S_0[\mathbf{S}^a(\tau)] - \frac{\beta^2 J^2}{2} \int_0^1 d\tau d\tau' Q(\tau - \tau') \sum_a \mathbf{S}^a(\tau) \cdot \mathbf{S}^a(\tau') - \beta^2 J^2 \sum_{a < b} Q_{ab} \int_0^1 d\tau \mathbf{S}^a(\tau) \int_0^1 d\tau' \mathbf{S}^b(\tau'). \quad (27)$$

We now need to specify an ansatz for the matrix Q_{ab} which allows for analytic continuation to non-integer matrix dimensions.

1.3 Replica symmetry breaking

1.3.1 Recursive construction

We use Parisi's replica symmetry breaking (RSB) ansatz for the matrix Q_{ab} . The matrix Q^{RSB_k} at the k^{th} stage of RSB is defined by the choice of two sequences: $(q_p)_{p=0..k}$ and $(m_p)_{p=0..k}$, the latter being strictly decreasing, with $m_0 = n$. It is built "from the inside out" according to the following prescription:

1. $Q_k^{\text{RSB}_k} = (q_k - q_{k-1})U_{m_k}$;
2. $\forall p \in [0, k-1], Q_p^{\text{RSB}_k} = \text{diag}_{m_p/m_{p+1}}(Q_{p+1}^{\text{RSB}_k}) + (q_p - q_{p-1})U_{m_p}$;
3. $Q_0^{\text{RSB}_k} \equiv Q^{\text{RSB}_k}$.

Here U_m is the matrix of size m filled with ones of size, $\text{diag}_r(A)$ is the matrix with r times the block A on the diagonal, and we set $q_{-1} = 0$. We note that this construction places q_k instead of 0 on the diagonal, and the corresponding term needs to be subtracted in the end. In the classical

case, the local Hamiltonian at the k^{th} stage of RSB is therefore

$$H_{\text{loc}}^{\text{RSB}_k} = nq_k \frac{\beta J^2 S^2}{2} - \frac{\beta J^2}{2} \sum_{ab} (Q^{\text{RSB}_k})^{ab} \mathbf{S}^a \cdot \mathbf{S}^b, \quad (28)$$

which we may write as

$$H_{\text{loc}}^{\text{RSB}_k} = \sum_a H_k[\mathbf{S}_a] - \frac{\beta J^2}{2} \sum_{ab} (Q^{\text{RSB}_k})^{ab} \mathbf{S}^a \cdot \mathbf{S}^b. \quad (29)$$

In the quantum case, we introduce the notation $\bar{\mathbf{S}} \equiv \int_0^1 d\tau \mathbf{S}(\tau)$. Then, the local action at the k^{th} stage of RSB is

$$\mathcal{S}_{\text{loc}}^{\text{RSB}_k} = \sum_a \mathcal{S}_0[\mathbf{S}^a(\tau)] - \int_0^1 d\tau d\tau' \frac{\beta^2 J^2 (Q(\tau' - \tau) - q_k)}{2} \sum_a \mathbf{S}^a(\tau) \cdot \mathbf{S}^a(\tau') - \frac{\beta^2 J^2}{2} \sum_{ab} (Q^{\text{RSB}_k})^{ab} \bar{\mathbf{S}}^a \cdot \bar{\mathbf{S}}^b. \quad (30)$$

For simplicity, we denote

$$\mathcal{S}_{\text{loc}}^{\text{RSB}_k} = \sum_a \mathcal{S}_k[\mathbf{S}^a(\tau)] - \frac{\beta^2 J^2}{2} \sum_{ab} (Q^{\text{RSB}_k})^{ab} \bar{\mathbf{S}}^a \cdot \bar{\mathbf{S}}^b. \quad (31)$$

We now establish a recursion between the local partition functions Z_{loc} at steps p and $p+1$ of the recursive construction. We use the quantum notation, but the relation will be identical in the classical case. At step p the local partition function under an external field \mathbf{h} reads:

$$Z_p^{\text{RSB}_k}(\mathbf{h}) = \int \prod_a [D\mathbf{S}^a] \exp \left[- \sum_a \mathcal{S}_k[\{\mathbf{S}^a\}] + \frac{\beta^2 J^2}{2} \sum_{ab} (Q_p^{\text{RSB}_k})^{ab} \bar{\mathbf{S}}^a \cdot \bar{\mathbf{S}}^b + \beta \mathbf{h} \sum_a \bar{\mathbf{S}}^a \right]. \quad (32)$$

We note that \mathbf{h} is introduced only as an auxiliary term, and we will set $\mathbf{h} = 0$ in the end. In particular it does not represent an actual external field applied on the initial system: the matrix Q_{ab} would then no longer be rotationally invariant. At the first step ($p = k$), we find

$$\begin{aligned} Z_k^{\text{RSB}_k}(\mathbf{h}) &= \int \prod_a [D\mathbf{S}^a] \exp \left[- \sum_{a=1}^{m_k} \mathcal{S}_k[\{\mathbf{S}^a\}] + \frac{\beta^2 J^2}{2} (q_k - q_{k-1}) \left(\sum_{a=1}^{m_k} \bar{\mathbf{S}}^a \right)^2 + \beta \mathbf{h} \sum_{a=1}^{m_k} \bar{\mathbf{S}}^a \right] \\ &= \int d\mathbf{h}_k \mathbb{G}(\mathbf{h}_k | 2J^2(q_k - q_{k-1})) \left(\int [D\mathbf{S}] e^{-\mathcal{S}_k[\mathbf{S}] + \beta(\mathbf{h} + \mathbf{h}_k)\bar{\mathbf{S}}} \right)^{m_k} \\ &\equiv \int d\mathbf{h}_k \mathbb{G}(\mathbf{h}_k | 2J^2(q_k - q_{k-1})) z_k(\mathbf{h} + \mathbf{h}_k)^{m_k}. \end{aligned} \quad (33)$$

At step p , we may consider separately the effect of the two terms in $Q_p^{\text{RSB}_k}$:

$$\begin{aligned} Z_p^{\text{RSB}_k}(\mathbf{h}) &= \int \prod_a [D\mathbf{S}^a] \exp \left[- \sum_{a=1}^{m_p} \mathcal{S}_k[\{\mathbf{S}^a\}] + \frac{\beta^2 J^2}{2} (q_p - q_{p-1}) \left(\sum_{a=1}^{m_p} \bar{\mathbf{S}}^a \right)^2 \right. \\ &\quad \left. + \frac{\beta^2 J^2}{2} \sum_{\alpha=1}^{m_p/m_{p+1}} \sum_{a,b \in \alpha} (Q_{p+1}^{\text{RSB}_k})^{ab} \bar{\mathbf{S}}^a \cdot \bar{\mathbf{S}}^b + \beta \mathbf{h} \sum_{a=1}^{m_p} \bar{\mathbf{S}}^a \right]. \end{aligned} \quad (34)$$

Here, α labels the blocks of the matrix $Q_p^{\text{RSB}_k}$. After a Hubbard-Stratonovitch transformation on the squared sum, we find the recurrence relation

$$Z_p^{\text{RSB}_k}(\mathbf{h}) = \int d\mathbf{h}_p \mathbb{G}(\mathbf{h}_p | 2J^2(q_p - q_{p-1})) \left[Z_{p+1}^{\text{RSB}_k}(\mathbf{h} + \mathbf{h}_p) \right]^{m_p/m_{p+1}}. \quad (35)$$

1.3.2 Limit $n \rightarrow 0, k \rightarrow \infty$

We now take the simultaneous limit $n \rightarrow 0$ and $k \rightarrow \infty$, keeping $m_k = 1$. Then, m_p becomes a continuous variable x between 0 and 1, and $q_p \rightarrow q(x)$, such that $m_p \rightarrow x$. $q(x)$ is the Parisi order parameter. The corresponding limit of the recurrence relation (35) may be taken if one uses the formal identity

$$\left[\exp \left(\frac{1}{2} v \nabla^2 \right) \cdot f \right] (\mathbf{h}) = \int d\mathbf{h}' \mathbb{G}(\mathbf{h}'|v) f(\mathbf{h} + \mathbf{h}'), \quad (36)$$

that holds for any sufficiently regular function f . $Z_p^{\text{RSB}_k}(\mathbf{h})$ then becomes a continuous function $\zeta(x, \mathbf{h})$, satisfying

$$\zeta(x - dx, \mathbf{h}) = \exp \left(\frac{1}{2} J^2 dq(x) \nabla^2 \right) \zeta(x, \mathbf{h})^{1-dx/x} \quad (37)$$

This may be recast into a partial differential equation:

$$\frac{\partial \zeta}{\partial x} = -\frac{1}{2} J^2 \frac{dq}{dx} \nabla^2 \zeta + \frac{1}{x} \zeta \log \zeta, \quad (38)$$

with boundary condition $\zeta(1, h) = z_\infty(\mathbf{h})$ as defined below. At this point, a distinction needs to be made between the classical and the quantum case. In the classical case, the "single-replica" part of the local Hamiltonian H_k does not depend on the spin. We may hence split it off in the partition function, so that applying Eq. (35) at $p = 0$ yields

$$\lim_{n \rightarrow 0} \frac{1}{n} \log Z_{\text{loc}}^{\text{Cl}} = -\frac{\beta^2 J^2 S^2}{2} q(1) + \int d\mathbf{h} \mathbb{G}(\mathbf{h}|2J^2 q(0)) \lim_{x \rightarrow 0} \left[\frac{1}{x} \log \zeta(x, \mathbf{h}) \right], \quad (39)$$

and the boundary condition is explicitly

$$z_\infty^{\text{Cl}}(\mathbf{h}) = \int d\mathbf{S} e^{-\beta H_\infty(\mathbf{h})} = 2\pi \int_0^\pi d\theta \sin \theta e^{-\beta h S \cos \theta} = \frac{2\pi}{\beta h S} (e^{\beta h S} - e^{-\beta h S}). \quad (40)$$

We may define $\phi(x, \mathbf{h}) \equiv (1/x) \log \zeta(x, \mathbf{h})$, which satisfies

$$\frac{\partial \phi}{\partial x} = -\frac{1}{2} J^2 \frac{dq}{dx} \left(\nabla^2 \phi + x (\nabla \phi)^2 \right). \quad (41)$$

We also anticipate that $q(0) = 0$, so that the Gaussian in Eq. (39) becomes a δ function.

Then, introducing our results into Eq. (23) the free energy of the classical Heisenberg spin glass is given by

$$f = -\frac{\beta J^2 S^4}{4\ell} - \frac{\ell \beta J^2}{4} \int_0^1 dx q(x)^2 + \frac{\beta J^2 S^2}{2} q(1) - \frac{1}{\beta} \phi(0, 0), \quad (42)$$

where $\phi(x, h)$ satisfies Eq. (41) with $\phi(1, \mathbf{h}) = \log z_\infty^{\text{Cl}}(\mathbf{h})$.

We have used that, with the RSB ansatz [7],

$$\lim_{n \rightarrow 0} \sum_{a < b} Q_{ab}^2 = -\frac{1}{2} \int_0^1 dx q(x)^2. \quad (43)$$

This provides the solution of the classical spin glass problem given a function $q(x)$.

In the quantum case, the single-replica part of the action cannot be simplified and we obtain

$$\lim_{n \rightarrow 0} \frac{1}{n} \log Z_{\text{loc}}^{\text{Q}} = \int d\mathbf{h} \mathbb{G}(\mathbf{h}|2J^2 q(0)) \lim_{x \rightarrow 0} \left[\frac{1}{x} \log \zeta(x, \mathbf{h}) \right], \quad (44)$$

and

$$z_\infty^{\mathcal{Q}}(\mathbf{h}) = \int [D\mathbf{S}] e^{-\mathcal{S}_\infty[\mathbf{S}(\tau), \mathbf{h}]}, \quad (45)$$

with

$$\mathcal{S}_\infty(\mathbf{h}) = \mathcal{S}_0[\mathbf{S}(\tau)] - \int_0^1 d\tau d\tau' \frac{\beta^2 J^2 (Q(\tau - \tau') - q(1))}{2} \mathbf{S}(\tau) \cdot \mathbf{S}(\tau') + \beta \mathbf{h} \cdot \mathbf{S} \quad (46)$$

Then, introducing our results into Eq. (25) the free energy of the quantum Heisenberg spin glass is given by

$$f = \frac{\ell \beta J^2}{4} \left[\int_0^1 d\tau Q(\tau)^2 - \int_0^1 dx q(x)^2 \right] - \frac{1}{\beta} \phi(0, 0), \quad (47)$$

where $\phi(x, h)$ satisfies Eq. (41) with $\phi(1, \mathbf{h}) = \log z_\infty^{\mathcal{Q}}(\mathbf{h})$.

This provides the solution of the quantum spin glass problem given $q(x)$ and $Q(\tau)$.

1.3.3 Local observables and two point functions

We now determine the functions $q(x)$ and $Q(\tau)$ by applying the RSB ansatz to the self-consistency conditions in Eqs. (24) and (26). We go back to the recursive construction in 1.3.1 and consider the observable $R^a(\tau, \tau') = \mathbf{S}^a(\tau) \mathbf{S}^a(\tau')$, which is local in replica space. For every τ, τ' , we define the quantity $R_p^{\text{RSB}_k}(\mathbf{h})$, which corresponds to the average value of R computed with the matrix Q^{RSB_k} built up to step p . $R_p^{\text{RSB}_k}$ is only slightly different from $Z_p^{\text{RSB}_k}$: indeed, at a given step, only one of the blocks is perturbed by the insertion of R , while the others are not. Therefore, one has the recurrence relation

$$R_p^{\text{RSB}_k}(\mathbf{h}) = \int d\mathbf{h}_p \mathbb{G}(\mathbf{h}_p | 2J^2(q_p - q_{p-1})) \frac{R_{p+1}^{\text{RSB}_k}(\mathbf{h} + \mathbf{h}_p) Z_{p+1}^{\text{RSB}_k}(\mathbf{h} + \mathbf{h}_p)^{m_p/m_{p+1}}}{Z_p^{\text{RSB}_k}(\mathbf{h})}. \quad (48)$$

The situation is slightly different for an observable that is non-local in replica space, in particular the spin-spin correlator $\langle \bar{\mathbf{S}}^a \bar{\mathbf{S}}^b \rangle^{\text{RSB}_k}$. When k is sufficiently large, a and b are always in different blocks at k -RSB. If at step p they are still in different blocks, then $\langle \bar{\mathbf{S}}^a \bar{\mathbf{S}}^b \rangle_p^{\text{RSB}_k} = (\langle \bar{\mathbf{S}} \rangle_p^{\text{RSB}_k})^2$. Let p_0 be the first step where $\bar{\mathbf{S}}^a$ and $\bar{\mathbf{S}}^b$ are in the same block. Then for $p < p_0$, the spin-spin correlator satisfies the same recurrence relation as a local observable:

$$\langle \bar{\mathbf{S}}^a \bar{\mathbf{S}}^b \rangle_p^{\text{RSB}_k}(\mathbf{h}) = \int d\mathbf{h}_p \mathbb{G}(\mathbf{h}_p | 2J^2(q_p - q_{p-1})) \frac{\langle \bar{\mathbf{S}}^a \bar{\mathbf{S}}^b \rangle_{p+1}^{\text{RSB}_k}(\mathbf{h} + \mathbf{h}_p) Z_{p+1}^{\text{RSB}_k}(\mathbf{h} + \mathbf{h}_p)^{m_p/m_{p+1}}}{Z_p^{\text{RSB}_k}(\mathbf{h})}. \quad (49)$$

In the limit $n \rightarrow 0, k \rightarrow \infty$, $R_p^{\text{RSB}_k}(\mathbf{h})$ becomes a function $\rho(x, \mathbf{h})$, satisfying

$$\zeta(x - dx, \mathbf{h}) \rho(x - dx, \mathbf{h}) = \exp\left(\frac{1}{2} J^2 dq(x) \nabla^2\right) \rho(x, \mathbf{h}) \zeta(x, \mathbf{h})^{1-dx/x}. \quad (50)$$

The corresponding PDE is

$$\frac{\partial \rho}{\partial x} = -\frac{1}{2} J^2 \frac{dq}{dx} \left(\nabla^2 \rho + 2(\nabla \log \zeta) \cdot (\nabla \rho) \right), \quad (51)$$

with the boundary condition $\rho(1, \mathbf{h})_{\tau, \tau'} = \langle \mathbf{S}(\tau) \mathbf{S}(\tau') \rangle_{\infty, \mathbf{h}}$, where $\langle \cdot \rangle_{\infty, \mathbf{h}}$ is the mean value with respect to $H_\infty(\mathbf{h})$ or $\mathcal{S}_\infty(\mathbf{h})$. If we now define $\beta \mathbf{s}(x, \mathbf{h}) = (1/x) \nabla \log \zeta$, we find that it satisfies the same equation as ρ , with the boundary condition $\mathbf{s}(1, \mathbf{h}) = \langle \mathbf{S} \rangle_\infty$. Then ρ satisfies

$$\frac{\partial \rho}{\partial x} = -\frac{1}{2} J^2 \frac{dq}{dx} \left(\nabla^2 \rho + 2\beta \mathbf{s} \cdot \nabla \rho \right) \quad (52)$$

Using Eq. (48) with $p = 0$,

$$Q(\tau - \tau') = \int d\mathbf{h} \mathbb{G}(\mathbf{h} | 2J^2 q(0)) \rho(0, \mathbf{h})_{\tau, \tau'} = \rho(0, 0)_{\tau, \tau'}. \quad (53)$$

The spin-spin correlation function $\langle \mathbf{S}^a \mathbf{S}^b \rangle_p^{\text{RSB}_k}$ becomes a continuous function $\nu(y, x, \mathbf{h})$, where y is the continuum analogue of the index p_0 defined above. For $y < x$, ν satisfies Eq. (52), with the boundary condition $\nu(y = x, x, \mathbf{h}) = \mathbf{s}^2(x, \mathbf{h})$. The self-consistency conditions (24) and (26) become

$$q(x) = \frac{1}{\ell} \int d\mathbf{h} \mathbb{G}(\mathbf{h} | 2J^2 q(0)) \nu(0, x, \mathbf{h}) = \frac{1}{\ell} \nu(0, x, 0). \quad (54)$$

This completes in principle our solution of the spin glass problem. One only needs to compute the average magnetization and the time correlation function in a single spin problem governed by H_∞ or \mathcal{S}_∞ . This yields, through integration of Eq. (52), the functions $q(x)$ and $Q(\tau)$, which allow one in turn to compute the free energy, starting from the partition function associated with H_∞ or \mathcal{S}_∞ . However, these results are formulated much more conveniently by introducing the probability distribution of the local field.

1.3.4 Probability distribution of the local field

We introduce the probability distribution $\mathbb{P}(\mathbf{h})$ of the local field acting on the effective impurity problem. Let us define the function $P(x, \mathbf{h} | x', \mathbf{h}')$ as the solution of the "backward" eq. (52) with boundary condition $P(x', \mathbf{h} | x', \mathbf{h}') = \delta(\mathbf{h} - \mathbf{h}')$. For any $x' \geq x$, it has the Markovian property

$$P(x, \mathbf{h} | 1, \mathbf{h}'') = \int d\mathbf{h}' P(x, \mathbf{h} | x', \mathbf{h}') P(x', \mathbf{h}' | 1, \mathbf{h}''). \quad (55)$$

Differentiating with respect to x' yields

$$0 = \int d\mathbf{h}' [\partial_{x'} P(x, \mathbf{h} | x', \mathbf{h}') P(x', \mathbf{h}' | 1, \mathbf{h}'') + P(x, \mathbf{h} | x', \mathbf{h}') \partial_{x'} P(x', \mathbf{h}' | 1, \mathbf{h}'')], \quad (56)$$

and since P satisfies (52), we obtain

$$\begin{aligned} \int d\mathbf{h}' P(x', \mathbf{h}' | 1, \mathbf{h}'') \partial_{x'} P(x, \mathbf{h} | x', \mathbf{h}') = \\ - \int d\mathbf{h}' P(x, \mathbf{h} | x', \mathbf{h}') \frac{J^2}{2} \dot{q}(x') \left(\nabla_{\mathbf{h}'}^2 P(x', \mathbf{h}' | 1, \mathbf{h}'') + 2\beta x' (\mathbf{s} \cdot \nabla_{\mathbf{h}'}) P(x, \mathbf{h}' | 1, \mathbf{h}'') \right). \end{aligned} \quad (57)$$

Integrating by parts,

$$\begin{aligned} \int d\mathbf{h}' P(x', \mathbf{h}' | 1, \mathbf{h}'') \partial_{x'} P(x, \mathbf{h} | x', \mathbf{h}') = \\ \int d\mathbf{h}' P(x', \mathbf{h}' | 1, \mathbf{h}'') \frac{J^2}{2} \dot{q}(x') \left(\nabla_{\mathbf{h}'}^2 P(x, \mathbf{h} | x', \mathbf{h}') - 2\beta x' \nabla_{\mathbf{h}'} (\mathbf{s}(x', \mathbf{h}') \cdot P(x, \mathbf{h} | x', \mathbf{h}')) \right). \end{aligned} \quad (58)$$

Since this is true for any \mathbf{h}'' , $P(x, \mathbf{h} | x', \mathbf{h}')$ is found to satisfy the "forward" equation

$$\frac{\partial P}{\partial x'} = \frac{J^2}{2} \dot{q}(x') \left(\nabla_{\mathbf{h}'}^2 P - 2\beta x' \nabla_{\mathbf{h}'} (\mathbf{s} \cdot P) \right). \quad (59)$$

We now rewrite eq. (53) as

$$\langle R \rangle_{\mathcal{S}} = \int d\mathbf{h}' d\mathbf{h} \mathbb{G}(\mathbf{h} | 2J^2 q(0)) P(0, \mathbf{h} | 1, \mathbf{h}') \langle R \rangle_{\mathcal{S}_1(\mathbf{h}')} \equiv \int \mathbb{P}(1, \mathbf{h}') \langle R \rangle_{\mathcal{S}_1(\mathbf{h}')}, \quad (60)$$

having defined

$$\mathbb{P}(x', \mathbf{h}') = \int d\mathbf{h} \mathbb{G}(\mathbf{h} | 2J^2 q(0)) P(0, \mathbf{h} | x', \mathbf{h}'). \quad (61)$$

\mathbb{P} then satisfies eq. (59) with boundary condition $\mathbb{P}(0, \mathbf{h}) = \mathbb{G}(\mathbf{h} | 2J^2 q(0)) = \delta(\mathbf{h})$. Similarly, for the Parisi order parameter we find

$$q(x) = \frac{1}{\ell} \int d\mathbf{h} \mathbb{P}(x, \mathbf{h}) \mathbf{s}^2(x, \mathbf{h}) \quad (62)$$

1.3.5 Final formulation of the solution

We are now in position to formulate the solution in its final form.

We have reduced the solution of the fully connected Heisenberg spin glass problem to the solution of a single spin problem. It is governed in the classical case by the Hamiltonian $H_\infty(\mathbf{h}) = -\mathbf{h} \cdot \mathbf{S}$ and in the quantum case by the action

$$\mathcal{S}_\infty(\mathbf{h}) = \mathcal{S}_0[\mathbf{S}(\tau)] - \int_0^1 d\tau d\tau' \frac{\beta^2 J^2 (Q(\tau - \tau') - q(1))}{2} \mathbf{S}(\tau) \cdot \mathbf{S}(\tau') - \beta \int_0^1 \mathbf{h} \cdot \mathbf{S}(\tau). \quad (63)$$

The Parisi order parameter and local susceptibility are obtained as

$$q(x) = \frac{1}{\ell} \int d\mathbf{h} \mathbb{P}(x, \mathbf{h}) \mathbf{s}(x, \mathbf{h})^2 \quad \text{and} \quad Q(\tau) = \int d\mathbf{h} \mathbb{P}(1, \mathbf{h}) \langle \mathbf{TS}(\tau) \mathbf{S}(0) \rangle_{\infty, \mathbf{h}}, \quad (64)$$

where $\langle \cdot \rangle_{\infty, \mathbf{h}}$ denotes the mean value with respect to $H_\infty(\mathbf{h})$ or $\mathcal{S}_\infty(\mathbf{h})$. $\mathbb{P}(x, \mathbf{h})$ and $\mathbf{s}(x, \mathbf{h})$ are obtained by solving

$$\frac{\partial \mathbb{P}}{\partial x} = \frac{J^2}{2} \frac{dq}{dx} \left(\nabla^2 \mathbb{P} - 2\beta x \nabla(\mathbf{s} \cdot \mathbb{P}) \right) \quad \text{with} \quad \mathbb{P}(0, \mathbf{h}) = \delta(\mathbf{h}); \quad (65)$$

$$\frac{\partial \mathbf{s}}{\partial x} = -\frac{J^2}{2} \frac{dq}{dx} \left(\nabla^2 \mathbf{s} + 2\beta x (\mathbf{s} \cdot \nabla) \mathbf{s} \right) \quad \text{with} \quad \mathbf{s}(1, \mathbf{h}) = \langle \mathbf{S} \rangle_{\infty, \mathbf{h}}. \quad (66)$$

Once $q(x)$ and $Q(\tau)$ are known, the free energy can be evaluated according to Eqs. (42) and (47).

In practice, the local problem is solved trivially in the classical case:

$$\langle S \rangle_{\infty, \mathbf{h}} = S \left(\frac{1}{\tanh(\beta S h)} - \frac{1}{\beta S h} \right), \quad (67)$$

and the self-consistency needs only to be established between Eqs. (64) through (66). In the quantum case, the local problem is still a many-body problem, which can only be solved numerically. Moreover, the local action depends self-consistently on the observables $q(x)$ and $Q(\tau)$, so that convergence must be reached for two interconnected self-consistency loops (see Fig. 1 of the main text).

1.4 Internal energy

The internal energy per spin U/N can in principle be obtained by numerically differentiating the free energy with respect to temperature. However, it can be obtained in a more straightforward way by carrying out the differentiation analytically before replica symmetry breaking. Going back to Eqs. (9) and (16), we compute the internal energy as

$$\frac{U}{N} = -\frac{\partial(\beta f)}{\partial \beta} = -\lim_{n \rightarrow 0} \frac{1}{n} \frac{\partial \mathcal{F}[\{Q_{ab}^*\}]}{\partial \beta}. \quad (68)$$

Since the Q_{ab} were introduced as integration variables, they may be arbitrarily rescaled. If we define $\tilde{Q}_{ab} = \beta^2 J^2 Q_{ab}$, the "complicated" terms in Eq. (8) and (15) no longer have an explicit β dependence. We then obtain, in the classical case,

$$\frac{\partial \mathcal{F}_{\text{Cl}}}{\partial \beta} = -\frac{n\beta J^2 S^4}{2\ell} - \frac{\ell}{\beta^3 J^2} \sum_{a < b} \tilde{Q}_{ab}^2 = -\frac{n\beta J^2 S^4}{2\ell} - \ell \beta J^2 \sum_{a < b} Q_{ab}^2. \quad (69)$$

We then use the property

$$\lim_{n \rightarrow 0} \sum_{a < b} Q_{ab}^2 = -\frac{1}{2} \int_0^1 dx q(x)^2, \quad (70)$$

to obtain

$$\frac{U_{\text{Cl}}}{N} = -\frac{\beta J^2 S^4}{2\ell} \left(1 - \frac{\ell^2}{S^4} \int_0^1 dx q(x)^2 \right). \quad (71)$$

Similarly, in the quantum case,

$$\begin{aligned} \frac{\partial \mathcal{F}_Q}{\partial \beta} &= -\frac{n\ell}{2\beta^3 J^2} \int_0^1 d\tau d\tau' \tilde{Q}_{aa}(\tau, \tau')^2 - \frac{\ell}{\beta^3 J^2} \sum_{a < b} \tilde{Q}_{ab}^2 \\ &= -\frac{n\ell\beta J^2}{2} \int_0^1 d\tau d\tau' Q_{aa}(\tau, \tau')^2 - \ell\beta J^2 \sum_{a < b} Q_{ab}^2, \end{aligned} \quad (72)$$

so that

$$\frac{U_Q}{N} = -\frac{\ell\beta J^2}{2} \left(\int_0^1 d\tau Q(\tau)^2 - \int_0^1 dx q(x)^2 \right). \quad (73)$$

1.5 Doped quantum spin glass

Our solution is readily generalized to a "doped" Heisenberg spin glass model. Physically, the randomly-interacting spins are now being carried by electrons, which can hop between the sites of a fully connected lattice and experience an on-site repulsion U . The corresponding Hamiltonian is

$$H = H_0 + U \sum_i n_{i\uparrow} n_{i\downarrow} - \sum_{i < j} J_{ij} \bar{\mathbf{S}}_i \cdot \bar{\mathbf{S}}_j, \quad (74)$$

with $H_0 = -\sum_{ij,\sigma} (t_{ij} + \mu\delta_{ij}) c_{i\sigma}^\dagger c_{j\sigma}$. Here the $c_{i\sigma}$ and $c_{i\sigma}^\dagger$ are the electronic annihilation and creation operators, $\sigma = \uparrow, \downarrow$ labels the spin state, $n_{i\sigma} = c_{i\sigma}^\dagger c_{i\sigma}$ is the occupation number on site i , U is the on-site electron-electron interaction, μ is the chemical potential and the t_{ij} are hopping amplitudes, randomly distributed with variance t^2/N . The spins are defined in terms of the fermionic operators as $S_i^\alpha = (1/2) \sum_{\sigma, \sigma'} c_{i\sigma}^\dagger \sigma_{\sigma\sigma'}^\alpha c_{i\sigma'}$, with σ^α the Pauli matrices.

The solution of this model proceeds along the same steps as above, and here we only outline the main differences. We represent the partition function as a path integral over the Grassman variables $(c_{i\sigma}^\dagger(\tau), c_{i\sigma}(\tau))$:

$$Z = \int \prod_i [Dc_{i\sigma}^\dagger(\tau)][Dc_{i\sigma}(\tau)] e^{-\int_0^\beta d\tau \left[\sum_{i,\sigma} c_{i\sigma}^\dagger(\tau) \partial_\tau c_{i\sigma}(\tau) + H(\tau) \right]}. \quad (75)$$

Note that we now let the imaginary time run between 0 and β . We then compute $\overline{Z^n}$, with the disorder average now being carried out over both the couplings J_{ij} and the hoppings t_{ij} . The Hubbard-Stratonovitch transformation now introduces integration variables Q_{ab} and Δ_{ab} , that decouple respectively the spin-spin interaction term and the hopping term. Upon performing the relevant simplifications (for instance, the $\Delta_{a \neq b}$ vanish), and dropping indices for simplicity,

$$\overline{Z^n} \propto \int [DQ][D\Delta] \exp \left[-N \left\{ \int_0^\beta d\tau d\tau' \left(\frac{J^2(Q^{ab})^2}{4} + \frac{(\Delta^a)^2}{t^2} \right) - \log \int [Dc] e^{-\mathcal{S}_{\text{loc}}[Q, \Delta]} \right\} \right], \quad (76)$$

with

$$\begin{aligned} \mathcal{S}_{\text{loc}} &= \int_0^\beta d\tau \sum_{a\sigma} [c_\sigma^{a\dagger}(\tau) (\partial_\tau - \mu) c_\sigma^a(\tau) + U n_\uparrow^a(\tau) n_\downarrow^a(\tau)] + \dots \\ &+ \int_0^\beta d\tau d\tau' \sum_a \left[\Delta(\tau' - \tau) \sum_\sigma c_\sigma^{a\dagger}(\tau') c_\sigma^a(\tau) - \frac{J^2 Q(\tau' - \tau)}{2} \mathbf{S}^a(\tau) \cdot \mathbf{S}^a(\tau') \right] - J^2 \sum_{a < b} Q^{ab} \mathbf{S}^a(\tau) \cdot \mathbf{S}^b(\tau'). \end{aligned} \quad (77)$$

The saddle point equations read

$$\Delta(\tau) = t^2 G(\tau), \quad G(\tau) = -\langle \mathbf{T} c_\sigma^a(\tau) c_\sigma^{\dagger a}(0) \rangle; \quad (78)$$

$$Q(\tau - \tau') = \frac{1}{\ell} \langle \mathbf{T} \mathbf{S}^a(\tau) \cdot \mathbf{S}^a(\tau') \rangle_{S_{\text{loc}}}; \quad (79)$$

$$Q_{ab} = \frac{1}{\ell} \langle \mathbf{S}^a(\tau) \cdot \mathbf{S}^b(\tau) \rangle_{S_{\text{loc}}}. \quad (80)$$

Upon replica symmetry breaking, the original lattice problem is reduced to a self-consistent impurity problem, governed by the action

$$\begin{aligned} \mathcal{S}_\infty(\mathbf{h}) = & \int_0^\beta d\tau \sum_\sigma [c_\sigma^\dagger(\tau) (\partial_\tau - \mu) c_\sigma(\tau) + U n_\uparrow(\tau) n_\downarrow(\tau)] - \int_0^\beta d\tau \mathbf{h} \cdot \mathbf{S}(\tau) \\ & + \int_0^\beta d\tau d\tau' \left[\Delta(\tau' - \tau) \sum_\sigma c_\sigma^\dagger(\tau') c_\sigma(\tau) - \frac{J^2(Q(\tau' - \tau) - q(1))}{2} \mathbf{S}(\tau) \cdot \mathbf{S}(\tau') \right]. \end{aligned} \quad (81)$$

The self-consistency conditions read

$$q(x) = \frac{1}{\ell} \int d\mathbf{h} \mathbb{P}(x, \mathbf{h}) \mathbf{s}(x, \mathbf{h})^2, \quad Q(\tau) = \int d\mathbf{h} \mathbb{P}(1, \mathbf{h}) \langle \mathbf{T} \mathbf{S}(\tau) \mathbf{S}(0) \rangle_{\infty, \mathbf{h}}, \quad (82)$$

and

$$\Delta(\tau) = t^2 \int d\mathbf{h} \mathbb{P}(x, \mathbf{h}) \frac{1}{2} \sum_\sigma G_\sigma(\tau, \mathbf{h}), \quad \text{with} \quad G_\sigma(\tau) = -\langle \mathbf{T} c_\sigma(\tau) c_\sigma^\dagger(0) \rangle_{\infty, \mathbf{h}}. \quad (83)$$

$\mathbb{P}(x, \mathbf{h})$ and $\mathbf{s}(x, \mathbf{h})$ are obtained by solving Eqs. (65) and (66).

We note that we have used in Eq. (83) the spin-symmetrized Green's function $\bar{G}(\tau) = (G_\uparrow(\tau) + G_\downarrow(\tau))/2$. In the absence of an external magnetic field, it is equal to the Green's function of either spin. In the presence of a field \mathbf{h} , G_\uparrow and G_\downarrow depend on both the magnitude and direction of the \mathbf{h} , but \bar{G} depends only on $\|\mathbf{h}\|$.

Indeed, let us apply a unitary transformation U to the basis of spin states $\{|\sigma\rangle\}$. This defines new basis vectors $\{|\sigma'\rangle\}$. We may define creation and annihilation operators for spin up and spin down electrons in this new basis. They are given by

$$c_{\sigma'}^\dagger = \sum_{\sigma=\uparrow, \downarrow} U_{\sigma'\sigma} c_\sigma^\dagger \quad \text{and} \quad c_{\sigma'} = \sum_{\sigma=\uparrow, \downarrow} U_{\sigma'\sigma}^* c_\sigma \quad (84)$$

The spin up Green's function in the new basis is

$$G'_\uparrow(\tau) = -\langle (U_{\uparrow\uparrow}^* c_\uparrow(\tau) + U_{\uparrow\downarrow}^* c_\downarrow(\tau)) (U_{\uparrow\uparrow} c_\uparrow^\dagger(0) + U_{\uparrow\downarrow} c_\downarrow^\dagger(0)) \rangle \quad (85)$$

$$= |U_{\uparrow\uparrow}|^2 G_\uparrow(\tau) + |U_{\uparrow\downarrow}|^2 G_\downarrow(\tau) - U_{\uparrow\uparrow}^* U_{\uparrow\downarrow} \langle c_\uparrow(\tau) c_\downarrow^\dagger(0) \rangle - U_{\uparrow\uparrow} U_{\uparrow\downarrow}^* \langle c_\downarrow(\tau) c_\uparrow^\dagger(0) \rangle \quad (86)$$

Similarly,

$$G'_\downarrow(\tau) = -\langle (U_{\downarrow\uparrow}^* c_\uparrow(\tau) + U_{\downarrow\downarrow}^* c_\downarrow(\tau)) (U_{\downarrow\uparrow} c_\uparrow^\dagger(0) + U_{\downarrow\downarrow} c_\downarrow^\dagger(0)) \rangle \quad (87)$$

$$= |U_{\downarrow\uparrow}|^2 G_\uparrow(\tau) + |U_{\downarrow\downarrow}|^2 G_\downarrow(\tau) - U_{\downarrow\uparrow}^* U_{\downarrow\downarrow} \langle c_\uparrow(\tau) c_\downarrow^\dagger(0) \rangle - U_{\downarrow\uparrow} U_{\downarrow\downarrow}^* \langle c_\downarrow(\tau) c_\uparrow^\dagger(0) \rangle \quad (88)$$

Now, the unitarity of U imposes that $|U_{\uparrow\uparrow}|^2 + |U_{\uparrow\downarrow}|^2 = 1$ and $U_{\uparrow\uparrow} U_{\uparrow\downarrow}^* + U_{\uparrow\downarrow} U_{\downarrow\downarrow}^* = 0$, so that

$$G'_\uparrow(\tau) + G'_\downarrow(\tau) = G_\uparrow(\tau) + G_\downarrow(\tau). \quad (89)$$

The spin-symmetrized Green's function is thus rotationally-invariant even under an external magnetic field.

2 Numerical procedures

2.1 Solution of the Parisi equations

2.1.1 Integral equation formulation

The Parisi equations Eqs. (65) and (66) are non-linear partial differential equations that need to be solved numerically. We introduce the Green's function $G(x, \mathbf{h}|x', \mathbf{h}')$ of their linear part, which satisfies

$$\begin{cases} \frac{\partial G}{\partial x} = \frac{J^2}{2} \frac{dq}{dx} \nabla^2 G & \text{for } x \geq x' \\ \frac{\partial G}{\partial x} = -\frac{J^2}{2} \frac{dq}{dx} \nabla^2 G & \text{for } x \leq x' \end{cases}. \quad (90)$$

with $G(x', \mathbf{h}|x', \mathbf{h}') = \delta(\mathbf{h} - \mathbf{h}')$. G is simply a Gaussian:

$$G(x, \mathbf{h}|x', \mathbf{h}') = \frac{1}{[2\pi J^2 |q(x) - q(x')|]^{3/2}} \exp\left(-\frac{(\mathbf{h} - \mathbf{h}')^2}{2J^2 |q(x) - q(x')|}\right). \quad (91)$$

If we now treat the non-linear terms as source terms, Eqs. (65) and (66) can be formally integrated according to

$$\mathbb{P}(x, \mathbf{h}) = \frac{1}{(2\pi J^2 q(0))^{3/2}} e^{-h^2/2J^2 q(0)} - \beta J^2 \int_0^x dx' x' \dot{q}(x') \int d\mathbf{h}' G(x, \mathbf{h}|x', \mathbf{h}') \nabla(\mathbf{s} \cdot \mathbb{P})|_{x', \mathbf{h}'} \quad (92)$$

and

$$\mathbf{s}(x, \mathbf{h}) = \int d\mathbf{h}' G(x, \mathbf{h}|1, \mathbf{h}') \langle \mathbf{S} \rangle_{\infty, \mathbf{h}'} + \beta J^2 \int_x^1 dx' x' \dot{q}(x') \int d\mathbf{h}' G(x, \mathbf{h}|x', \mathbf{h}') (\mathbf{s} \cdot \nabla) \mathbf{s}|_{x', \mathbf{h}'} \quad (93)$$

We now use the fact that $\mathbf{s}(x, \mathbf{h})$ is always in the direction of \mathbf{h} : $\mathbf{s}(x, \mathbf{h}) = s(x, h) \hat{\mathbf{h}}$. Then,

$$\nabla(\mathbf{s} \cdot \mathbb{P})|_{x', \mathbf{h}'} = \frac{1}{h'^2} \frac{\partial(h'^2 s \mathbb{P})}{\partial h'} \quad (94)$$

and

$$(\mathbf{s} \cdot \nabla) \mathbf{s}|_{x', \mathbf{h}'} = s \frac{\partial s}{\partial h'} \hat{\mathbf{h}}'. \quad (95)$$

Hence, we may introduce angle-integrated Green's functions:

$$\begin{aligned} \bar{G}(x, h|x', h') &= (h')^2 \int d\hat{\mathbf{h}}' G(x, \mathbf{h}|x', \mathbf{h}') \\ &= \frac{1}{[2\pi J^2 |q(x) - q(x')|]^{1/2}} \frac{hh'}{h^2} \left[\exp\left(-\frac{(h-h')^2}{2J^2 |q(x) - q(x')|}\right) - \exp\left(-\frac{(h+h')^2}{2J^2 |q(x) - q(x')|}\right) \right]; \end{aligned} \quad (96)$$

$$\begin{aligned} \bar{G}_s(x, h|x', h') &= (h')^2 \int d\hat{\mathbf{h}}' G(x, \mathbf{h}|x', \mathbf{h}') (\hat{\mathbf{h}}' \cdot \hat{\mathbf{h}}) \\ &= \frac{1}{[2\pi J^2 |q(x) - q(x')|]^{1/2}} \frac{1}{h^2} \left[(J^2 |q(x) - q(x')| + hh') \exp\left(-\frac{(h+h')^2}{2J^2 |q(x) - q(x')|}\right) \right. \\ &\quad \left. + (hh' - J^2 |q(x) - q(x')|) \exp\left(-\frac{(h-h')^2}{2J^2 |q(x) - q(x')|}\right) \right]. \end{aligned} \quad (97)$$

Eqs. (92) and (93) then reduce to one-dimensional integral equations:

$$\mathbb{P}(x, h) = \frac{1}{(2\pi J^2 q(x))^{3/2}} e^{-h^2/2J^2 q(x)} - \beta J^2 \int_0^x dx' x' \dot{q}(x') \int dh' \bar{G}(x, h|x', h') \frac{1}{h'^2} \frac{\partial(h'^2 s \mathbb{P})}{\partial h'} \quad (98)$$

and

$$s(x, h) = \int dh' \bar{G}_s(x, h|1, h') \langle S \rangle_{\infty, \mathbf{h}'} + \beta J^2 \int_x^1 dx' x' \dot{q}(x') \int dh' \bar{G}_s(x, h|x', h') s \frac{\partial s}{\partial h'} \Big|_{x', h'}. \quad (99)$$

2.1.2 Numerical procedure

Our solver code for Eqs. (98) and (99), written in Python, is available on Zenodo [12]. The variable x is discretized, and Eqs. (98) and (99) are solved on successive x points. We typically use 128 to 256 x points in the region where $q(x)$ is non-constant. When $q(x)$ and $q(x')$ are very close, the Green's functions $\overline{G}(x, h|x', h')$ are strongly peaked around $h = h'$. However, the result of the convolution varies much more slowly as a function of h . Therefore, we sample h' on a very fine grid (typically 20000 points) and h on a much coarser Chebyshev grid (typically 256 points), and then use barycentric interpolation to obtain the result of the convolution on the fine grid for the next integration step.

When the non-linear term is large (typically, when $q(x)$ is large), the numerical integration procedure is unstable. Indeed, at step n , the non-linear term contains a contribution from the n^{th} numerical derivative of the initial condition, which develops an oscillatory instability with a frequency on the order of the Chebyshev grid spacing. As long as the grid is much finer than the structure in $\mathbb{P}(x, h)$ and $s(x, h)$, the spurious oscillations may be filtered out. We use Savitzky-Golay filtering, which amounts to splitting the h interval into panels, and fitting $\mathbb{P}(x, h)$ or $s(x, h)$ with a second degree polynomial in h on each of the panels. The panel size is determined adaptively, as a fraction of the value of h where the non-linear term has a maximum. With this procedure, and given our level of discretization, the filtered-out part is $\lesssim 10^{-5}$ of the remainder at every x step, which roughly sets the precision level of our solver. We further check that the normalization $\int_0^\infty 4\pi h^2 \mathbb{P}(x, h) dh = 1$ and the sum rule [8]

$$1 - \frac{\ell}{S^2} \int_0^1 dx q(x) = T \quad (100)$$

in the classical case are satisfied to a precision better than 10^{-4} after self-consistency has been reached.

2.2 Solution of the quantum impurity problem

We solve the quantum impurity problem defined by the action in Eq. (81), and its restriction in Eq. (63), by using a continuous-time Monte Carlo procedure based on a hybridization expansion in the segment picture (CTSEG algorithm) [9, 10]. Our quantum Monte Carlo code, based on the TRIQS library, is available on GitHub [11]. Briefly, the algorithm is based on the double expansion of the hybridization (Δ) and spin-spin interaction (Q) terms. A configuration is defined by the order of the expansion and by the choice of points in imaginary time. Several possible updates or "moves" are defined for the configuration, which are accepted or rejected according to the Metropolis prescription. Further details of our implementation will be described elsewhere.

2.3 General solution procedure

2.3.1 Classical case

In the classical case, the magnetization $\langle \mathbf{S} \rangle_{\infty, \mathbf{h}}$ is known analytically and does not depend on the spin glass parameters. Therefore, we start from an initial guess for $q(x)$ and iteratively solve Eqs. (66) and (65) until convergence. As self-consistency is approached, $q(x)$ develops a singularity: $q(x) = q(1)$ for $x > x_c$. Yet, our numerical solution cannot produce a singularity in the mathematical sense. Two procedures can be envisioned for finding the breakpoint x_c .

1. We may apply a threshold to dq/dx . Concretely, once a new $q(x)$ has been determined from Eq. (64), we enforce that if $q(1) - q(x) < \epsilon$, $q(x) = q(1)$, with typically $\epsilon = 10^{-5}$, on the order of our solver's accuracy. This will result in the breakpoint moving as the solution is iterated, and eventually converging.

2. We may iterate the equations until convergence for a range of fixed values of x_c , and then choose the x_c for which the sum rule in Eq. (100) is most accurately satisfied.

We found that procedure 1 converges in a reasonable number of iterations at low temperatures $T/J \leq 0.04$, while procedure 2 is required for higher temperatures. At zero temperature, since x_c/T logarithmically diverges as $T \rightarrow 0$, there is no breakpoint in the finite interval of x/T in which we solve the equations.

2.3.2 Quantum case

In the quantum case, the magnetization $\langle \mathbf{S} \rangle_{\infty, \mathbf{h}}$ is obtained by solving the action in Eq. (81) or (63) with quantum Monte Carlo for a range of values of h . Furthermore, the action depends on the spin glass parameters and must be updated until self-consistency is reached. We start from an initial guess for $q(x)$ and $Q(\tau)$ (and $\Delta(\tau)$ in the doped case), and determine $\langle \mathbf{S} \rangle_{\infty, \mathbf{h}}$ (as well as the spin-spin correlation function, and possibly the electron Green's function) on the impurity, for typically 30 values of h sampled on a Chebyshev grid. The observables at arbitrary values of h are then inferred by barycentric interpolation. Then, given $\langle \mathbf{S} \rangle_{\infty, \mathbf{h}}$, Eqs. (66) and (65) are iterated N times. An arbitrarily large value of N is not necessarily best for rapid convergence of the whole self-consistent procedure; we found empirically that $N = 5$ is adequate. Procedure 1 (defined above) was sufficient to obtain reasonable convergence of the breakpoint. Once $q(x)$ and $\mathbb{P}(h)$ are obtained, we determine the $Q(\tau)$ and $\Delta(\tau)$ that define a new impurity action, and repeat the procedure until convergence of $q(x)$, $Q(\tau)$ and $\Delta(\tau)$.

The Parisi equations (66) and (65) can be solved directly at zero temperature, but not the quantum impurity problem. However, the input for the Parisi equations is only the magnetization, which we find to be almost converged with temperature for $\beta J > 100$ (Fig. S5). We use the magnetization obtained at the lowest accessible temperature $\beta J = 200$ as an input for the zero-temperature Parisi equations.

3 Supplementary figures

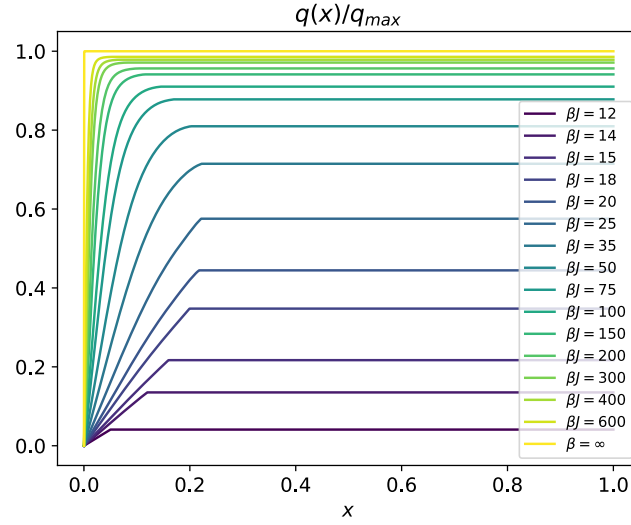


FIGURE S1: Parisi order parameter $q(x)$ for the classical Heisenberg spin glass, for a range of temperature values.

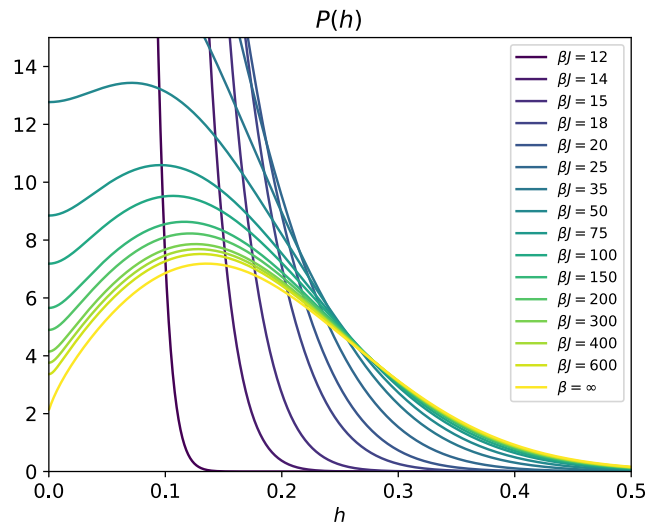


FIGURE S2: Local field probability distribution $\mathbb{P}(h)$ for the classical Heisenberg spin glass, for a range of temperature values.

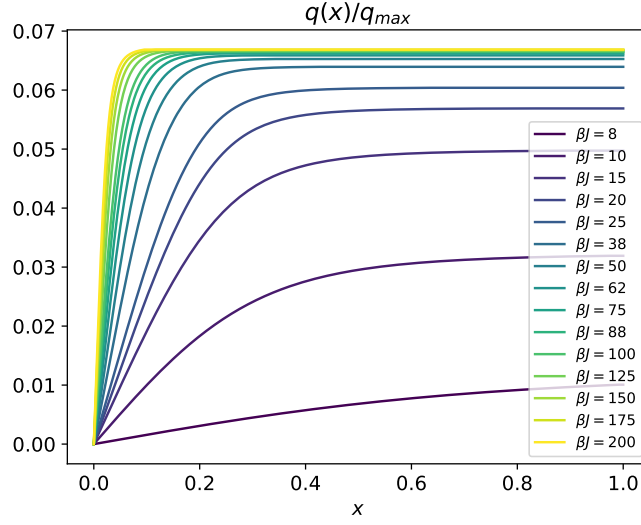


FIGURE S3: Parisi order parameter $q(x)$ for the quantum Heisenberg spin glass, for a range of temperature values. We did not attempt to reach convergence for the breakpoint at high temperature ($\beta J < 50$), as its position has a negligible influence on the other properties of the spin glass (particularly, the scaling of $Q(\tau)$).

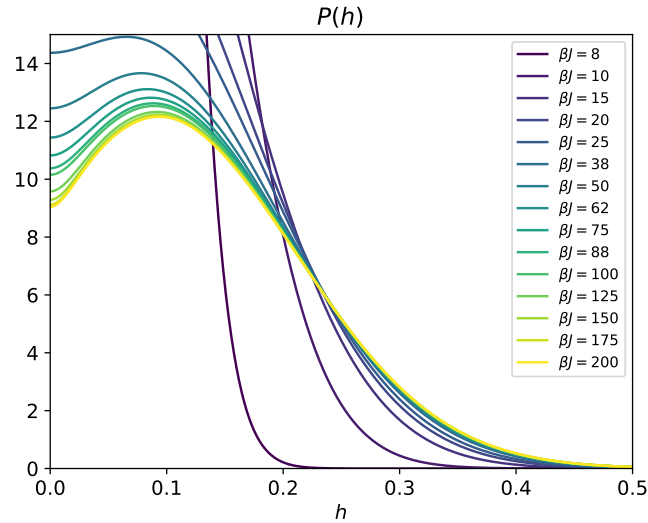


FIGURE S4: Local field probability distribution $\mathbb{P}(h)$ for the quantum Heisenberg spin glass, for a range of temperature values.

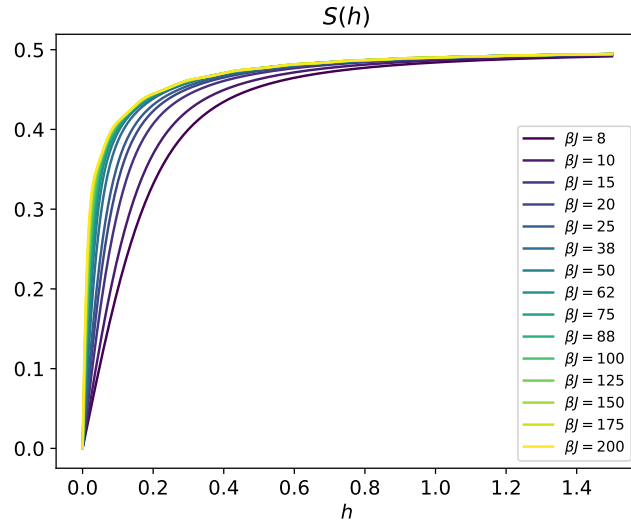


FIGURE S5: Magnetization $\langle S \rangle_{\infty, h}$ of the quantum Heisenberg spin glass, for a range of temperature values.

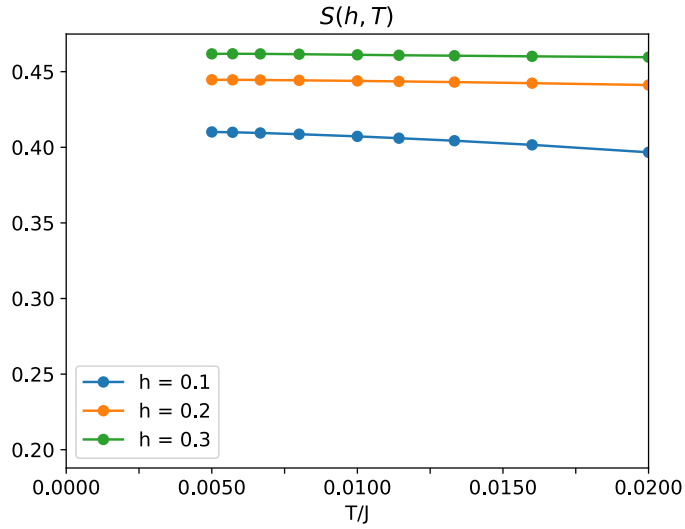


FIGURE S6: Magnetization $\langle S \rangle_{\infty, h}$ versus temperature, for three magnetic field values. At the lowest accessible temperatures, the magnetization is almost converged to its zero temperature shape.

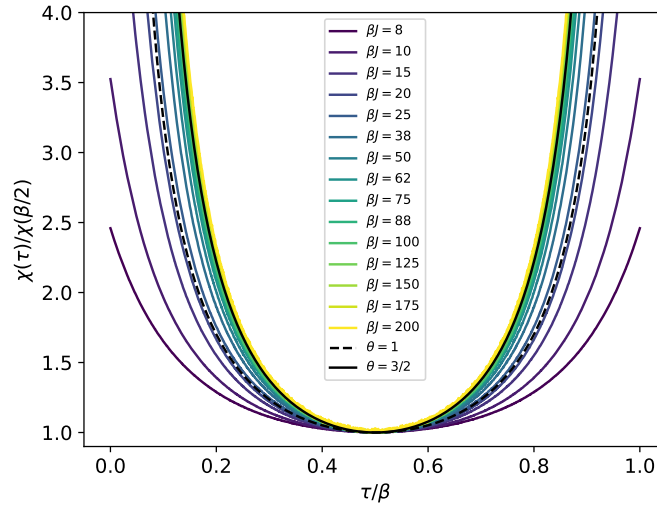


FIGURE S7: Rescaled spin susceptibility in the quantum spin glass phase $\chi(\tau)/\chi(\beta/2)$, for a range of temperature values. It is well described by the conformal scaling form $\chi(\tau)/\chi(\beta/2) = 1/\sin(\pi\tau/\beta)^\theta$. The scaling functions are plotted for $\theta = 1$ and $\theta = 3/2$ (black lines).

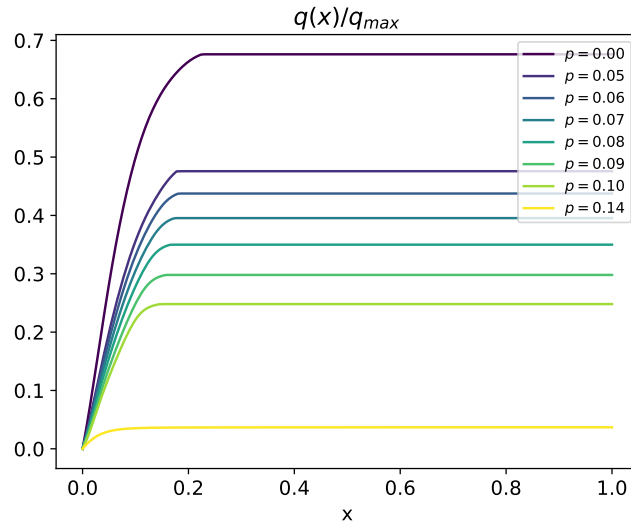


FIGURE S8: Parisi order parameter $q(x)$ for the doped Heisenberg spin glass at $\beta J = 50$, for a range of values of the doping p .

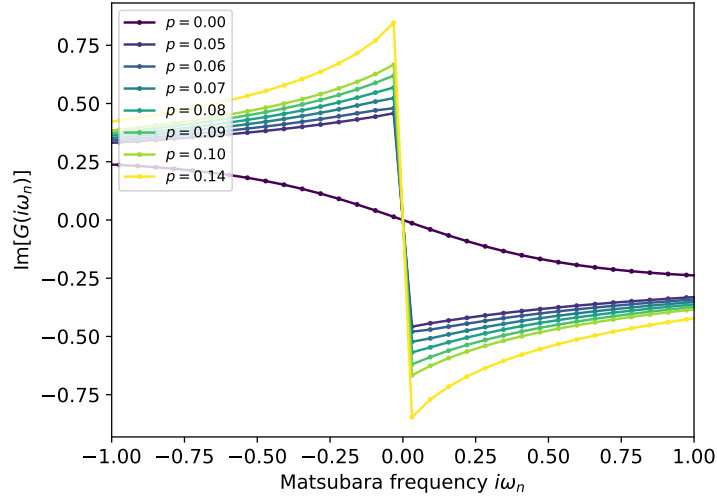


FIGURE S9: Imaginary part of the electron Green's function for the doped Heisenberg spin glass at $\beta J = 50$, for a range of values of the doping p .

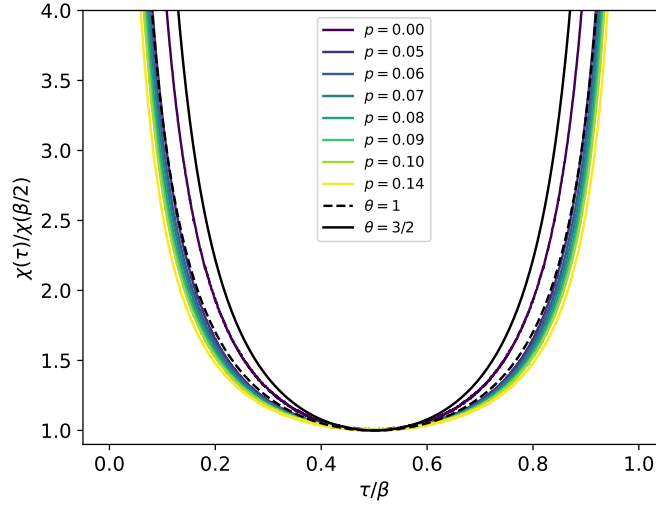


FIGURE S10: Rescaled spin susceptibility in the metallic spin glass phase $\chi(\tau)/\chi(\beta/2)$, at $\beta J = 50$, for a range of values of the doping p . It is reasonably described by the conformal scaling form $\chi(\tau)/\chi(\beta/2) = 1/\sin(\pi\tau/\beta)^\theta$. The scaling functions are plotted for $\theta = 1$ and $\theta = 3/2$ (black lines).

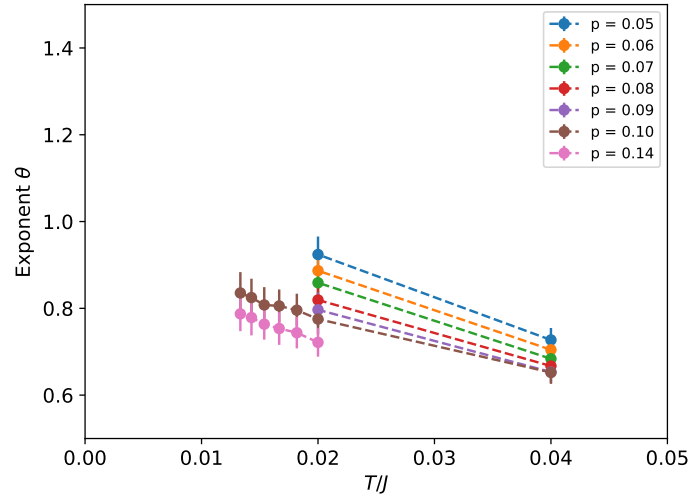


FIGURE S11: Scaling exponent θ , as a function of temperature in the metallic spin glass phase, for a range of values of the doping p .

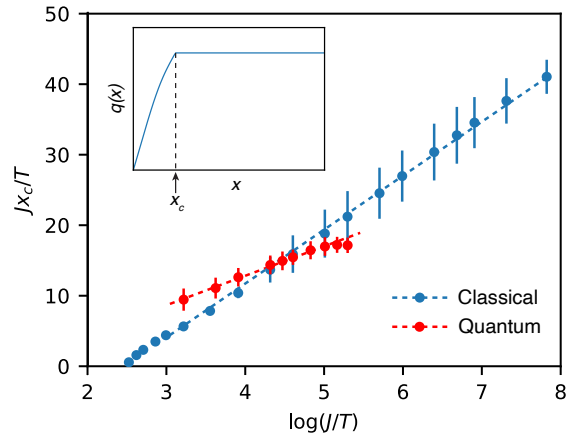


FIGURE S12: Breakpoint $x_c(T)$ vs T . $x_c(T)/T$ is a characteristic inverse energy scale governing the distribution of free energies of excited states. It scales logarithmically with T in both the classical and the quantum case. Dashed lines are guides to the eye. Inset: definition of the breakpoint x_c ($q(x > x_c) = q(1)$).

References

- [1] Sherrington, D. & Kirkpatrick, S. Solvable model of a spin-glass. *Physical Review Letters* **35**, 1792–1796 (1975).
- [2] Bray, A. J. & Moore, M. A. Replica theory of quantum spin glasses. *Journal of Physics C: Solid State Physics* **13**, L655 (1980).
- [3] Parisi, G. A sequence of approximated solutions to the S–K model for spin glasses. *Journal of Physics A: Mathematical and General* **13**, L115–L121 (1980).
- [4] Duplantier, B. Comment on Parisi’s equation for the SK model for spin glasses. *Journal of Physics A: General Physics* **14**, 283–285 (1981).
- [5] Andreanov, A. & Müller, M. Long-range quantum ising spin glasses at T=0: Gapless collective excitations and universality. *Physical Review Letters* **109**, 177201 (2012).
- [6] Kiss, A., Zaránd, G. & Lovas, I. Exact Solution for the Transverse Field Sherrington-Kirkpatrick Spin Glass Model with Continuous-Time Quantum Monte Carlo Method (2023). ArXiv:2306.07337 [cond-mat].
- [7] Gabay, M., Garel, T. & De Dominicis, C. Symmetry breaking a la Parisi in the n-component SK model of a spin glass. *Journal of Physics C: Solid State Physics* **15**, 7165–7180 (1982).
- [8] Crisanti, A. & Rizzo, T. Analysis of the infinite-replica symmetry breaking solution of the Sherrington-Kirkpatrick model. *Physical Review E* **65**, 046137 (2002).
- [9] Otsuki, J. Spin-boson coupling in continuous-time quantum Monte Carlo. *Physical Review B - Condensed Matter and Materials Physics* **87**, 125102 (2013).
- [10] Ayrál, T. PhD thesis. Nonlocal Coulomb interactions and electronic correlations: novel many-body approaches. Chapter 11. (2015).
- [11] https://github.com/TRIQS/ctseg_J
- [12] DOI: 10.5281/zenodo.10475973